Applied Radiation and Isotopes 69 (2011) 1830–1833

Contents lists available at ScienceDirect

Applied Radiation and Isotopes

journal homepage: www.elsevier.com/locate/apradiso

A phantom experiment for the evaluation of whole body exposure during BNCT using cyclotron-based epithermal neutron source (C-BENS)

T. Tsukamoto [a,*], H. Tanaka [b], H. Yoshinaga [b], T. Mitsumoto [c], A. Maruhashi [b], K. Ono [b], Y. Sakurai [b]

[a] Graduate School of Engineering, Kyoto University, Yoshida Honmachi, Sakyo-ku, Kyoto 606-8501, Japan
[b] Research Reactor Institute, Kyoto University, Asashiro-nishi 2-1010, Kumatori-cho, Osaka 590-0494, Japan
[c] Sumitomo Heavy Industries, Ltd., Osaki 2-1-1, Shinagawa, Tokyo 141-6025, Japan

ARTICLE INFO

Available online 21 March 2011

Keywords:
Cyclotron-based epithermal neutron source
Whole body exposure
Water phantom
Dose equivalent

ABSTRACT

At Kyoto University Research Reactor Institute (KURRI), cyclotron-based epithermal neutron source was installed in December 2008, and the supplementary construction works have been performed. As of December 2010, the various irradiation characteristics important for BNCT were mostly evaluated. The whole body exposure during BNCT medical irradiation is one of the important characteristics.

In this article, measurements of absorbed dose for thermal and fast neutrons and gamma-ray at ten positions corresponding to important organs are reported.

1. Introduction

At KURRI, cyclotron-based epithermal neutron source (C-BENS) was installed in December 2008, and neutron generation test was begun in March 2009. C-BENS consists of a cyclotron accelerator that can produce 1 mA, 30 MeV protons, a beam transport system with a neutron production beryllium target and the moderator for reducing the neutron energy from high energy up to 28 MeV to epithermal energy (Tanaka et al., 2009a). As of December 2010, the various irradiation characteristics important for BNCT, physical characteristics test and biological characteristics test using cell and mice were mostly evaluated. It was confirmed that the epithermal neutron beam intensity is about twice larger than that of heavy water neutron irradiation facility (HWNIF) of Kyoto University Reactor (KUR) (Sakurai and Kobayashi , 2002). However, fast neutron energy generated by beryllium target of C-BENS was higher than that of HWNIF. Hence, it is necessary to evaluate the whole body exposure caused by fast neutrons during medical BNCT irradiation.

To experimentally evaluate absorbed dose in whole human body, a water-filled phantom modified for whole human body was prepared. The measurements of thermal and fast neutron flux using neutron activation foils, and gamma-ray dose using thermo-luminescent dosimeters (TLDs) were performed. In this article, the evaluations of absorbed dose based on the measurement results at the locations of important organs are reported.

2. Material and methods

2.1. A human whole-body phantom

The human whole-body phantom is 170 cm in height, and consists of some rectangular acrylic-resin cases filled with water as shown in Fig. 1.

Thermal neutron flux was measured with neutron activation foil method using bare gold foils and cadmium-covered gold foils. The gold foils are 10 mm in diameter with the thickness of 0.05 mm. The fast neutron flux over the energy of 0.5 MeV was determined with the activity of indium foils. The indium foils are 20 mm in diameter with the thickness of 0.10 mm. Gamma-ray dose was measured by using TLDs. TLDs were made of beryllium oxide sealing in quartz cell in order to reduce the sensitivity for neutrons. The gold foils and TLDs were placed at ten positions: (1) brain, (2) thyroid, (3) esophagus, (4) bone marrow, (5) lung, (6) stomach, (7) liver, (8) colon, (9) bladder and (10) gonad. And the indium foils were positioned at nine positions except for the brain.

For the irradiation tests, it was assumed that a target volume was positioned at the depth of 2 cm from the left lateral surface of the head phantom and irradiated in the supine position. The phantom was attached to the beam aperture and the schematic layout of this experiment is shown in Fig. 2. The shape of the beam is circular and the size of irradiation field is 10 cm in diameter. After the irradiation, the activities of the gold and indium foils were measured with high-purity germanium detector (model GEM20P4, ORTEC).

2.2. Evaluation of the absorbed dose

In order to calculate the absorbed dose at ten positions, the neutron and gamma-ray sources at the surface of collimator,

* Corresponding author. Tel./fax: +81 72 451 2604.
E-mail addresses: t.tsukamoto@ft5.ecs.kyoto-u.ac.jp, tsukamoto3251@gmail.com (T. Tsukamoto).

0969-8043/$ - see front matter © 2011 Elsevier Ltd. All rights reserved.
doi:10.1016/j.apradiso.2011.03.013

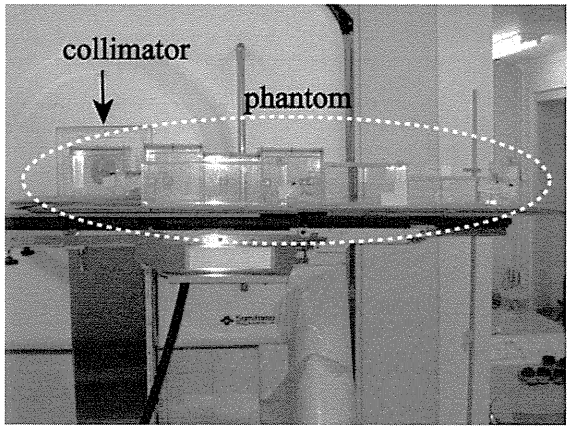

Fig. 1. Photograph of the experiments using a human whole-body phantom.

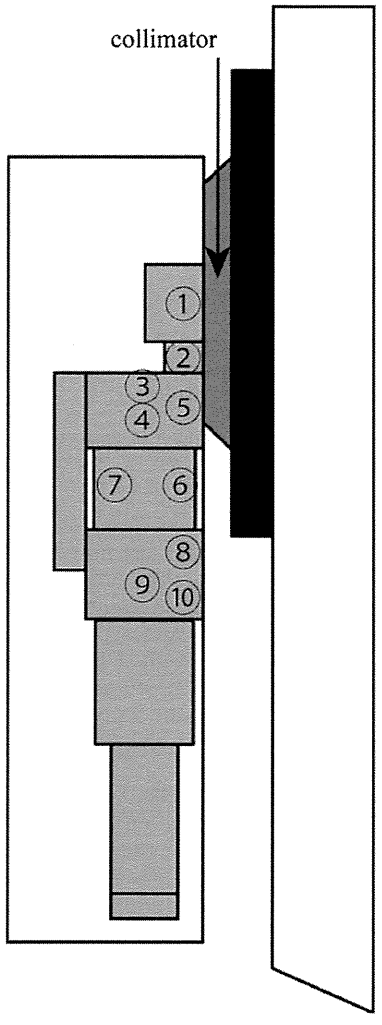

Fig. 2. Schematic layout of the irradiation tests in the supine position using a whole-body phantom. The numbers represent the assumed important organs 1, head; 2, thyroid; 3, esophagus; 4, bone marrow; 5, lung; 6, stomach; 7, liver; 8, colon; 9, bladder; and 10, gonad.

which were estimated by previous work (Tanaka et al., 2009a), were used. In the calculation, the collimator structures were modeled and the sources were modeled up to 150 cm in radius. The typical neutron spectra near the organs such as head, lung and liver are shown in Fig. 3. The calculated thermal and fast neutron absorbed doses were derived from the multiplication between the neutron spectrum calculated by MCNPX and kerma factors (Chadwick et al., 1999) considering the elemental components of each organ (ICRU, 1992).

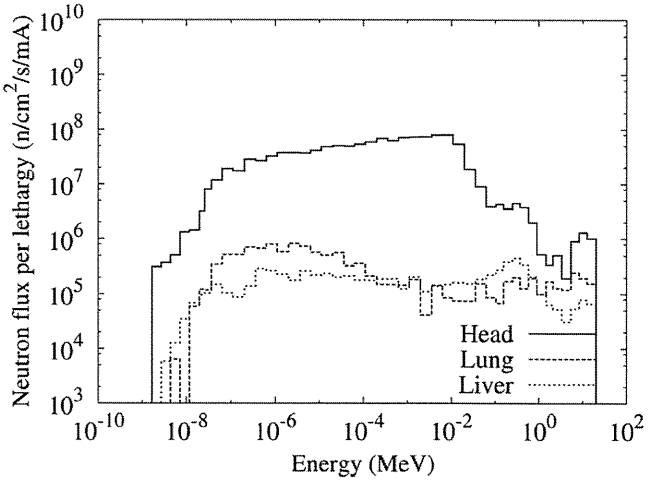

Fig. 3. Typical neutron energy spectra on the surface of head, and near lung and liver.

2.2.1. Absorbed dose for thermal neutrons

The calculated data of absorbed dose for thermal neutrons at each organ is normalized with the ratio of the measured and calculated data at the peak of the thermal neutron flux distribution in the head phantom. In this experiment, the activity at the peak of the thermal neutron distribution is highest compared with other position. Therefore, it is easy to obtain less statistical error. We select the location at the peak position to normalize.

On the other hand, to estimate the measured absorbed dose due to thermal neutrons, the calculated absorbed dose data was multiplied with the measured-to-calculated thermal neutron flux ratio.

2.2.2. Absorbed dose for fast neutrons

The calculated fast neutron absorbed dose at each organ is normalized with the ratio of the measured-to-calculated indium reaction rate at the position of thyroid in the neck phantom. In this experiment, the activity at the thyroid is highest compared with other position. Therefore, it is easy to obtain less statistical error. We select the location at the position of thyroid to normalize. The calculated reaction rate was derived from the multiplication of the energy spectrum and the cross-section data of JENDL/D-99.

On the other hand, to estimate the measured fast neutron absorbed dose, the calculated absorbed dose data was multiplied with the measured-to-calculated indium reaction rate ratio.

2.2.3. Gamma-ray dose

In order to estimate primary gamma-rays generated from the C-BENS components and secondary gamma-rays caused by the reactions between the neutrons and human body elements such as hydrogen, the calculations using F4 tally of MCNPX code without electron transport were performed separately with the neutron and gamma-ray sources. To derive the gamma ray dose, the flux to dose conversion factor was used. The measured primary and secondary gamma-ray doses are estimated by using the primary-to-secondary gamma-ray dose ratio calculated with

MCNPX. To estimate the calculated gamma-ray absorbed dose, data was normalized with the ratio of the measured and calculated data at the position of thyroid in the neck phantom.

3. Results and discussion

From the phantom experiments, it was confirmed that the peak of the thermal neutron flux distribution was at 2 cm depth from the left lateral surface in the head phantom, and the peak value for brain was almost 1.0×10^9 cm^{-2} s^{-1} per proton beam current of 1 mA. The thermal neutron flux of thyroid was 2.8×10^7 cm^{-2} s^{-1} per proton beam current of 1 mA and was much larger than that of the other organs. Because the thyroid was located near the target volume, the influence due to the thermal neutrons produced in brain was larger. In terms of the fast neutrons, ^{115}In(n,n′)^{115m}In reaction rate, the value of thyroid was 1.2×10^{-19} s^{-1} atom^{-1} per proton beam current of 1 mA and was more than twice larger than that of other organs. Fig. 4 shows the calculated neutron energy spectrum of lung which is one of the sensitive organs.

The gamma-ray absorbed dose in brain reached the maximum value at 2.7 cm depth from the left lateral surface. The absorbed dose for thyroid was about twice the values for the other organs.

Table 1 shows the calculated-to-measured absorbed dose ratios for thermal and fast neutrons and gamma-ray at the each organ. As a result, the measured thermal and fast neutron absorbed doses were in agreement with the calculated data within the factor of 0.4–2. The discrepancy between the calculated and measured data might be caused by the difference of angular distribution between calculation and experiment.

The estimated uncertainties of the measured thermal and fast neutron flux were 5% and 10%, respectively. The estimated uncertainties of the calculated thermal and fast neutron flux were less than 1%. The measured gamma-ray dose was in good agreement with the calculated data. The estimated uncertainties of the measured and calculated gamma-ray dose were 10% and 1%, respectively. Therefore, it is confirmed that the calculation for gamma-ray can simulate the measurements except in lung. The discrepancy between the calculated and measured gamma-ray doses for lung might be caused by the difference of experimental location of TLD compared with calculation location.

To evaluate the whole body exposure during BNCT medical irradiation, absorbed doses for thermal and fast neutrons were converted to relative biological effectiveness (RBE)-weighted dose. Fig. 5 shows the RBE-weighted dose for each organ. The irradiation time was assumed 40 min considering typical irradiation. Both of RBEs for thermal and fast neutrons are 3.0, respectively (Tanaka et al., 2009b). It was found that the gamma-ray dose was larger than the other dose components. At the position of thyroid, primary gamma-ray dose accounted for 45% of total dose and fast neutron dose accounted for 34%. And secondary gamma-ray dose accounted for 17% of total dose, because thyroid was located near the target volume with the distance of 13 cm, and thermal neutrons generated at the target was reduced during reaching into thyroid.

On the other hand, at other positions, the total dose of primary gamma-ray and fast neutron accounted for a large fraction of total dose. Hence it is guessed that the whole body exposure can be reduced by shielding the primary gamma-rays generated from the C-BENS components and fast neutrons.

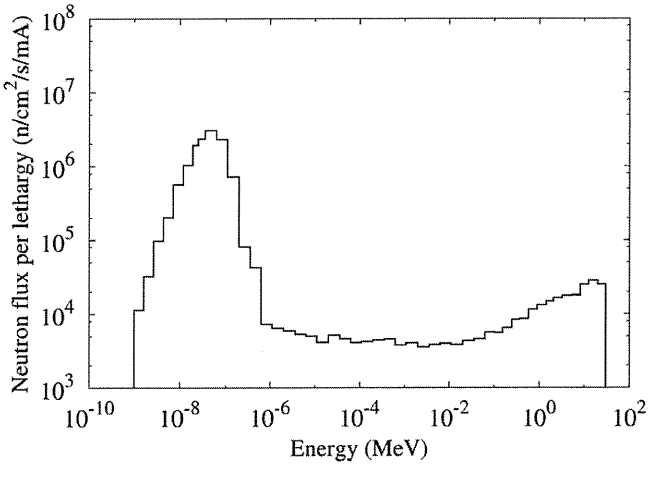

Fig. 4. Calculated neutron energy spectrum at the position of lung.

Table 1
Calculated-to-measured dose ratios for the thermal and fast neutrons and gamma-ray.

Organ	Ratio		
	Thermal neutron	Fast neutron	Gamma-ray
Thyroid	1.72	1.00	1.00
Esophagus	0.66	1.88	0.95
Bone marrow	0.59	1.34	0.96
Lung	1.11	0.89	1.52
Stomach	0.65	1.13	1.00
Liver	0.46	1.21	1.03
Colon	0.52	0.92	1.01
Bladder	0.43	0.86	0.93
Gonad	0.36	0.66	1.06

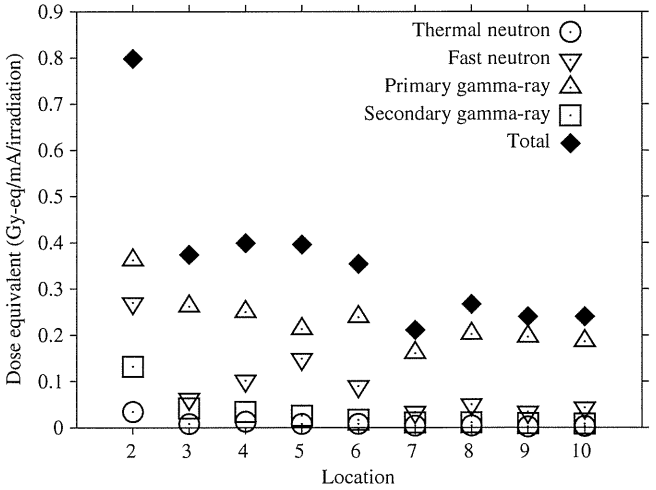

Fig. 5. RBE-weighted doses at locations of 2, thyroid; 3, esophagus; 4, bone marrow; 5, lung; 6, stomach; 7, liver; 8, colon; 9, bladder; and 10, gonad.

4. Conclusions

The whole body exposure was experimentally evaluated using the activation foils for thermal and fast neutrons and TLDs for gamma-rays. It is confirmed that the calculated MCNPX simulation results for whole body exposure were in agreement with the measured data within the factor of 0.4–2. It was also found that the primary gamma-ray dose and fast neutron dose were main components of the whole body exposure. Based on this research, the additional shields, polyethylene containing LiF and lead plate, were already set outside the aperture in the gap between a

patient and C-BENS to reduce primary gamma-ray and fast neutron dose. The shielding also has halved the thermal neutron fluence and dose.

References

Chadwick, M., Barschall, H., Caswell, R., DeLuca, P., Hale, G., Jones, D., MacFarlane, R., Meulders, J., Schuhmacher, H., Schrewe, U., Wambersie, A., Young, P., 1999. A consistent set of neutron kerma coefficients from thermal to 150 MeV for biologically important materials. Med. Phys. 26 (6), 974–991.

ICRU, 1992. Photon, electron, proton, and neutron interaction data for body tissues, ICRU Report 46, Bethesda, MD.

Sakurai, Y., Kobayashi, T., 2002. The medical-irradiation characteristics for neutron capture therapy at the heavy water neutron irradiation facility of Kyoto University Research Reactor. Med. Phys. 29 (10), 2328–2337.

Tanaka, H., Sakurai, Y., Suzuki, M., Masunaga, S., Kinashi, Y., Kashino, G., Liu, Y., Mitsumoto, T., Yajima, S., Tsutsui, H., Maruhashi, A., Ono, K., 2009a. Characteristics comparison between a cyclotron-based neutron source and KUR-HWNIF for boron neutron capture therapy. Nucl. Instrum. Methods B 267, 1970–1977.

Tanaka, H., Sakurai, Y., Suzuki, M., Takata, T., Masunaga, S., Kinashi, Y., Kashino, G., Liu, Y., Mitsumoto, T., Yajima, S., Tsutsui, H., Takada, M., Maruhashi, A., Ono, K., 2009b. Improvement of dose distribution in phantom by using epithermal neutron source based on the Be(p,n) reaction using a 30 MeV proton cyclotron accelerator. Appl. Radiat. Isot. 67, S258–S261 (13th International congress on neutron capture therapy BNCT: a new option against cancer).

Cancer Science
The official journal of the Japanese Cancer Association

Phase II study of erlotinib plus gemcitabine in Japanese patients with unresectable pancreatic cancer

Takuji Okusaka,[1,14] Junji Furuse,[2,3] Akihiro Funakoshi,[4] Tatsuya Ioka,[5] Kenji Yamao,[6] Shinichi Ohkawa,[7] Narikazu Boku,[8] Yoshito Komatsu,[9] Shoji Nakamori,[10] Haruo Iguchi,[11] Tetsuhide Ito,[12] Kazuhiko Nakagawa[13] and Kohei Nakachi[2]

[1]National Cancer Center Hospital, Tokyo; [2]National Cancer Center Hospital East, Kashiwa; [3]Kyorin University School of Medicine, Tokyo; [4]National Kyushu Cancer Center, Fukuoka; [5]Osaka Medical Center for Cancer and Cardiovascular Diseases, Osaka; [6]Aichi Cancer Center Hospital, Nagoya; [7]Kanagawa Cancer Center Hospital, Yokohama; [8]Shizuoka Cancer Center, Shizuoka; [9]Hokkaido University Hospital, Sapporo; [10]National Hospital Organization Osaka National Hospital, Osaka; [11]National Hospital Organization Shikoku Cancer Center, Ehime; [12]Kyushu University, Fukuoka; [13]Kinki University School of Medicine, Osaka, Japan

(Received April 1, 2010/Revised October 16, 2010/Accepted November 11, 2010/Accepted manuscript online November 26, 2010/Article first published online December 22, 2010)

Erlotinib combined with gemcitabine has not been evaluated in Japanese patients with unresectable pancreatic cancer. This two-step phase II study assessed the safety and pharmacokinetics of erlotinib 100 mg/day (oral) plus gemcitabine 1000 mg/m^2 (i.v. days 1, 8, 15) in a 28-day cycle in the first step, and efficacy and safety in the second step. The primary end-point was safety. One hundred and seven patients were enrolled (first step, n = 6; second step, n = 101). The most common adverse event was RASH (compiled using the preferred terms rash, acne, exfoliative rash, dermatitis acneiform, erythema, eczema, dermatitis and pustular rash) in 93.4% of patients. One treatment-related death occurred. While interstitial lung disease-like events were reported in nine patients (8.5%; grade 1/2/3, 3.8/2.8/1.9%), all patients recovered or improved. The median overall survival, the 1-year survival rate and median progression-free survival were 9.23 months, 33.0% and 3.48 months, respectively. The overall response and disease control rates were 20.3% and 50.0%, respectively. In Japanese patients with unresectable pancreatic cancer, erlotinib plus gemcitabine had acceptable toxicity and efficacy that was not inferior to that seen in Western patients. (*Cancer Sci* 2011; 102: 425–431)

Approximately 232 000 individuals are diagnosed with pancreatic cancer worldwide each year, with an annual death rate estimated at 227 000.[1] In Japan, approximately 22 000 new cases were reported in 2005.[2] Furthermore, data from 2007 show that around 24 000 individuals in Japan died from pancreatic cancer, making this tumor type the fifth leading cause of cancer-related death.[3] The majority of pancreatic cancer cases are diagnosed at an unresectable stage when prognosis is extremely poor.

Current treatment for advanced pancreatic cancer is based on systemic chemotherapy with gemcitabine. Single-agent gemcitabine has been shown to extend median overall survival (OS) to 5.65 months in chemonaïve patients compared with 4.41 months in patients who received fluorouracil.[4] Addition of other cytotoxic agents to gemcitabine has not demonstrated survival benefits over gemcitabine alone.[5–13] The potential of combining gemcitabine with biological agents in patients with advanced pancreatic cancer has also been evaluated in several phase III studies, but these trials failed to show a survival benefit.[14–19]

Epidermal growth factor receptor (EGFR)-mediated signaling is associated with various cellular processes, and the dysregulation of these processes is common in tumorigenesis.[20,21] Furthermore, EGFR is overexpressed in many tumors and its overexpression is often associated with poor prognosis.[22–26] EGFR tyrosine-kinase inhibitors (TKI, such as erlotinib) are used in the treatment of various types of solid tumors.

Erlotinib has demonstrated antitumor activity in pancreatic cell lines[27] and was subsequently assessed as a potential therapeutic agent in pancreatic cancer. In the PA.3 study (n = 569), the risk of death with erlotinib plus gemcitabine was reduced by 18% versus gemcitabine alone (hazard ratio [HR], 0.82; 95% confidence interval [CI], 0.69–0.99; P = 0.038 after adjustment for stratification factors), with a median OS of 6.24 months *vs* 5.91 months, respectively. Erlotinib plus gemcitabine combination therapy provided significant improvements in the 1-year survival rate (23% *vs* 17%; P = 0.023) and progression-free survival (PFS; HR 0.77; 95% CI, 0.64–0.92; P = 0.004).[28] As a result, this combination was approved for use in pancreatic cancer in many countries.

In Japanese patients with non-small-cell lung cancer (NSCLC), a phase II study has specifically shown that erlotinib monotherapy is well tolerated and has promising antitumor activity.[29] However, there are no data on the use of erlotinib combined with gemcitabine in Japanese patients with pancreatic cancer. This phase II study evaluated the safety and efficacy of erlotinib in combination with gemcitabine in Japanese patients with unresectable locally advanced or metastatic pancreatic cancer.

Methods

Patients. Patients aged 20–80 years with histological/cytological evidence of unresectable locally advanced or metastatic adenocarcinoma/adenosquamous carcinoma of the pancreas were eligible for inclusion in the present study. Patients were required to have an Eastern Cooperative Oncology Group (ECOG) performance status (PS) of 0–2, adequate hematological, renal and hepatic function and a life expectancy of at least 2 months. No more than one prior regimen for pancreatic cancer was permitted. Patients who had received prior gemcitabine and/or a TKI were excluded from participation, as were those who had previously been exposed to a human epidermal growth factor receptor 2 (HER2) or EGFR inhibitor. Other key

[14]To whom correspondence should be addressed.
E-mail: tokusaka@ncc.go.jp
Clinical trial registry: JAPIC Clinical Trials Information (see links below). http://rctportal.niph.go.jp/examDetail.php?center=3&center_seq=698 http://www.clinicaltrials.jp/user/cteDetail.jsp?clinicalTrialId=839&language=ja. Trial registration number: JapicCTI-060337.

doi: 10.1111/j.1349-7006.2010.01810.x

exclusion criteria were: symptomatic cerebral metastases; a concurrent lung disorder (such as idiopathic pulmonary fibrosis, interstitial lung disease [ILD] or pneumoconiosis); concurrent or previous drug-induced pneumonia; or a history of radiation to the chest.

The study complied with the Declaration of Helsinki and Good Clinical Practice guidelines. Informed consent was obtained from all patients, and the protocol was approved by ethics committees at all participating institutions.

Study design and treatment. This was a phase II, multicentre, open-label, two-step study. In the first step, six patients were enrolled into the study and treated with oral erlotinib 100 mg/day on days 3–28, plus i.v. gemcitabine 1000 mg/m^2 on days 1, 8 and 15 in a 28-day cycle. The starting doses of erlotinib and gemcitabine were chosen in reference to the PA.3 study. Dose-limiting toxicities (DLT) were assessed in these study participants using the National Cancer Institute Common Terminology Criteria for Adverse Events v3.0 (NCI-CTCAE, National Cancer Institute, Bethesda, MD, USA). Dose-limiting toxicities were defined in conformity to the P1b study as follows:[30] (i) grade 4 decrease (i.e. to <500/mm^3) in neutrophil count >5 days; (ii) grade ≥3 decrease (i.e. to <1000/mm^3) in neutrophil count with associated fever (≥38.5°C); (iii) grade 4 decrease in platelet count (i.e. to <25 000/mm^3); (iv) any grade ILD; (v) grade 4 elevation of alanine transaminase (ALT)/aspartate transaminase (AST) levels, or grade 3 elevation of ALT/AST levels >7 days; (vi) grade ≥3 non-hematological toxicity (excluding rash, hyperglycemia, γ-GTP and events that were judged to be transient/had no effect on study continuation); and (vii) dose-reduction/interruption required due to persistent adverse events (AE), which meant that the second cycle could not be started.

If treatment-related DLT occurred in no more than two of the six patients, transition to the second step of the study was permissible with approval of the Data Safety and Monitoring Committee (DSMC). If DLT occurred in three or more patients, transition to the second step was limited to those cases that were judged to be safe for this study after the DSMC had evaluated the safety data of the patients with a DLT. In the second step, it was planned that 94 patients would be treated with the same dose as the first step. Treatment was continued until disease progression, death, unacceptable toxicity or patient/investigator request.

The primary end-point of the study was safety, with secondary end-points including OS, 1-year survival rate, PFS, overall response rate (ORR), disease control rate (DCR = complete response [CR] + partial response [PR] + stable disease), pharmacokinetics (PK) and correlation of *EGFR* mutation status with outcomes.

Toxicity evaluation. Adverse events were monitored and graded using NCI-CTCAE v3.0. Clinical and laboratory assessments were conducted throughout the study. Adverse events prespecified in the study to be monitored carefully were rash, diarrhea, vomiting, liver dysfunction and ILD-like events. Chest X-ray examination to assess pulmonary toxicity was conducted weekly until week 4 and every 2 weeks thereafter. In addition, chest computed tomography (CT) scan was performed every 4 weeks. The DSMC reviewed the images and clinical data associated with all potential ILD-like events. All ILD-like events were reported to be serious AE (SAE), regardless of the grade.

Efficacy evaluation. The tumor response was assessed using Response Evaluation Criteria in Solid Tumors (RECIST) in patients who had at least one measurable target lesion. Tumors were measured using computed tomography (CT) at baseline and on day 22 of every two cycles thereafter. Median PFS, ORR and DCR were estimated by the extramural review. The relationship between efficacy and the severity of RASH (compiled using the preferred terms rash, acne, exfoliative rash, dermatitis acneiform, erythema, eczema, dermatitis and pustular rash) was also examined.

Pharmacokinetic evaluation. Pharmacokinetic evaluation of erlotinib and its O-desmethylated metabolite (OSI-420) was performed in the six patients enrolled in the first step of the study. Venous blood samples were taken prior to erlotinib dosing on day 3 and day 8 of cycle 1 at 0.5, 1, 2, 4, 6, 8 and 24 h after erlotinib administration. Samples were also taken prior to gemcitabine infusion on days 1 and 8 at 0.5, 0.75, 1, 1.5, 2.5 and 4.5 h after dosing.

The plasma concentrations of erlotinib, OSI-420 and gemcitabine were measured by liquid chromatography, tandem mass spectrometry (LC-MS-MS). The LC-MS-MS analytical methods have been described previously.[31,32] Derived PK parameters included the maximum plasma drug concentration (C_{max}), time to C_{max} (t_{max}), area under the plasma drug concentration-time curve to the last plasma sample (AUC_{last}), terminal half-life ($t_{½}$) and oral clearance (Cl/F).

Biomarker analysis. *EGFR* mutations were assessed in patients with available tumor tissue specimens, which were formalin fixed and paraffin embedded. Samples were analyzed at a central laboratory where DNA was extracted and exons 18–21 sequenced using a nested PCR.

Statistical analysis. Progression-free survival and OS were estimated using the Kaplan–Meier method in all patients who received at least one dose of the study treatment, with 95% CI for the median duration calculated using Greenwood's formula. The Clopper–Pearson method was used to calculate the 95% CI around the ORR, DCR and AE rate. Multivariate analyses were performed for the occurrence of ILD-like events using the logistic regression model. Baseline characteristics investigated for this analysis included gender, age, lung metastasis, emphysema and various baseline laboratory values. The target enrollment was 100 patients, as this was required to evaluate the safety of erlotinib.

Results

Patient characteristics. Between December 2006 and October 2007, a total of 107 patients were enrolled (first step, n = 6; second step, n = 101) from 12 institutions (Fig. 1). One patient who enrolled into the second step did not receive treatment due to deterioration in PS prior to the start of treatment. A total of 106 patients were evaluable for safety (safety population, full analysis set).

The patient demographics and baseline characteristics are shown in Table 1. The median age was 62 years (range, 36–78) and 52.8% of patients were male. Almost all patients were chemonaïve (95.3%). The majority (75.5%) of patients had an ECOG PS of 0 and most (83.0%) had metastatic disease. Over half (63.2%) of the patients had a history of current or past smoking.

Toxicity and dose modifications. The median duration of erlotinib exposure was 102.5 days and its median dose intensity was 100.0 mg/day, with the majority of patients (78.3%) receiving more than 90% of the relative dose intensity. The median duration of gemcitabine treatment was 4.0 cycles and its median dose intensity was 688.0 mg/m^2 per week, with approximately half of the patients (51.4%) receiving more than 90% of the relative dose intensity.

As only one patient had a DLT (grade 3 diarrhea) in the first step, the second step of the study was initiated. One hundred and six patients received at least one dose of erlotinib; these patients were assessable for toxicity. Treatment-related AE and treatment-related changes in laboratory values are summarized in Table 2; most of these were mild to moderate in severity. The most frequently reported AE was RASH, which occurred in

doi: 10.1111/j.1349-7006.2010.01810.x

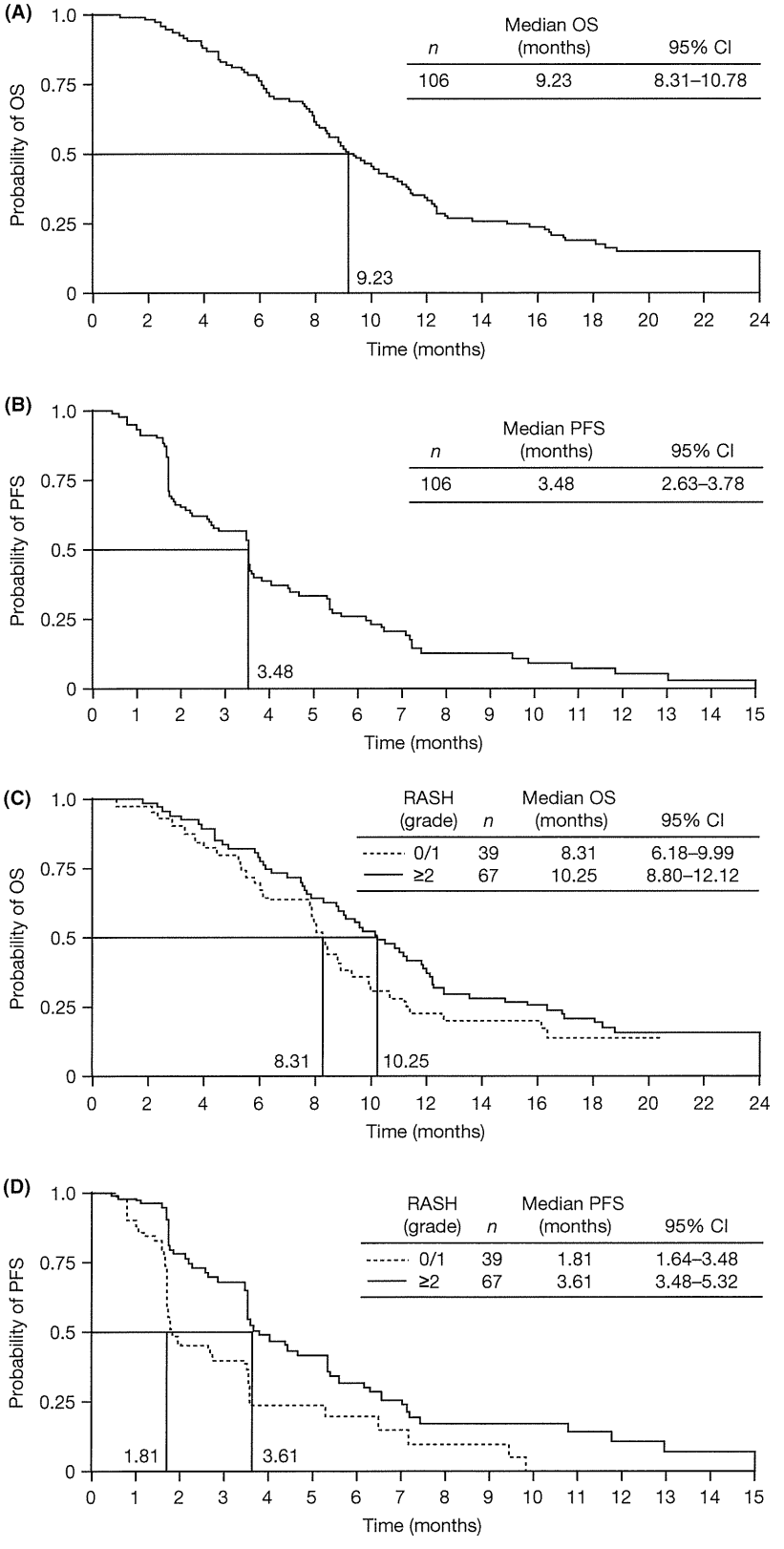

Fig. 1. Kaplan–Meier estimates of (A) overall survival (OS) and (B) progression-free survival (PFS) in the study population (n = 106); (C) OS and (D) PFS according to the severity of RASH (grade ≤1 [n = 39] *vs* grade ≥2 [n = 67]). RASH is a composite of the terms: rash, acne, exfoliative rash, dermatitis acneiform, erythema, eczema, dermatitis and pustular rash. CI, confidence interval.

Table 1. Baseline characteristics and demographics (n = 106)

Characteristic	
Median age (range) (years)	62 (36–78)
Gender, n (%)	
Male	56 (52.8)
Female	50 (47.2)
Median bodyweight (range) (kg)	52.3 (33.1–95.0)
Smoking history,† n (%)	
Never smoker	39 (36.8)
Past smoker	37 (34.9)
Current smoker	30 (28.3)
ECOG PS, n (%)	
0	80 (75.5)
1	26 (24.5)
2	0 (0)
Disease status, n (%)	
Metastatic	88 (83.0)
Locally advanced	18 (17.0)
Primary tumor identified, n (%)	92 (86.8)
Primary sites, n (%)	
Head	46 (43.4)
Body and tail	23 (21.7)
Body	22 (20.8)
Tail	10 (9.4)
Other	5 (4.7)‡
Biliary drainage, n (%)	19 (17.9)
Sites of distant metastases, n (%)	
Liver	56 (52.8)
Distant lymph nodes	39 (36.8)
Lung	17 (16.0)
Other	26 (24.5)
Prior lines of therapy, n (%)	
None	101 (95.3)
One regimen	5 (4.7)§
Median CA19-9 (range) (U/mL)	
Median	776 (0–435 000)
Median CEA (range) (ng/mL)	
Median	4.8 (0.6–1100.1)

†Never smoker, never/hardly smoked; past smoker, passage of at least 1 month since stopping smoking (at the time of registration); current smoker, smoked within 1 month (at the time of registration). ‡Whole of pancreas (n = 1); head and body (n = 3); other (n = 1). §Tegafur, gimeracil, oteracil potassium (S-1) (n = 3); 5-fluorouracil plus leucovorin (n = 2). CA 19–9, carbohydrate antigen 19–9; CEA, carcinoembryonic antigen; ECOG, Eastern Co-Operative Group.

93.4% of the patients; most cases were mild to moderate in severity (87.7%, grade ≤2; 5.7%, grade ≥3). Other common non-hematological AE included anorexia, pruritus, fatigue, nausea and diarrhea. Most patients experienced some degree of hematological toxicity, with grade 3 or 4 neutropenia (neutrophil decreased), leucopenia (white blood cell count decreased) and anemia (hemoglobin decreased) occurring in 34.9%, 29.2% and 14.2% of patients, respectively. Only one treatment-related death occurred (due to gastrointestinal hemorrhage), which was probably due to arterial bleeding caused by the invasion of the primary tumor into the gastrointestinal tract. Although the likelihood of this event being treatment-related was deemed remote, a causal relationship could not be completely excluded because the event occurred during the study treatment administration period.

Treatment-related SAE were reported in 26 (24.5%) patients. These included nine ILD-like events (8.5%), the majority of which (n = 7) were grade 1–2 in severity. Importantly, all of these nine patients recovered or improved, and four of these patients did so without any treatment for ILD-like events. Other

Table 2. Treatment-related adverse events occurring in >30% of patients treated with erlotinib and gemcitabine (n = 106)

	Any grade, n (%)	Grade 3, n (%)	Grade 4, n (%)
Non-hematological			
Rash	78 (73.6)	3 (2.8)	0 (0)
Anorexia	75 (70.8)	15 (14.2)	0 (0)
Pruritus	57 (53.8)	1 (0.9)	0 (0)
Fatigue	56 (52.8)	3 (2.8)	0 (0)
Nausea	56 (52.8)	6 (5.7)	0 (0)
Diarrhea	52 (49.1)	2 (1.9)	0 (0)
Dry skin	49 (46.2)	0 (0)	0 (0)
Stomatitis	38 (35.8)	0 (0)	0 (0)
Pyrexia	32 (30.2)	0 (0)	0 (0)
Hematological			
White blood cell count decreased	85 (80.2)	31 (29.2)	0 (0)
Platelet count decreased	77 (72.6)	9 (8.5)	0 (0)
Hemoglobin decreased	76 (71.7)	13 (12.3)	2 (1.9)
Hematocrit decreased	73 (68.9)	8 (7.5)	0 (0)
Neutrophil decreased	73 (68.9)	32 (30.2)	5 (4.7)
Red blood cell count decreased	72 (67.9)	8 (7.5)	0 (0)
ALT increased	59 (55.7)	10 (9.4)	0 (0)
AST increased	57 (53.8)	4 (3.8)	1 (0.9)
Weight decreased	53 (50.0)	3 (2.8)	0 (0)
Lymphocyte count decreased	46 (43.4)	14 (13.2)	0 (0)
Blood albumin decreased	35 (33.0)	0 (0)	0 (0)
Gamma-glutamyltransferase increased	35 (33.0)	12 (11.3)	1 (0.9)

ALT, alanine amino transferase; AST, aspartate amino transferase.

treatment-related SAE were anorexia (3.8%), vomiting, pyrexia and abnormal hepatic function (1.9% each). The baseline characteristics, treatment and outcomes of patients who developed treatment-related ILD-like events during the study are detailed in Table 3. The onset times of ILD-like events ranged from 7 to 187 days after the start of treatment. In these patients, a relatively long survival was observed (from 119 to 568+ days), and five patients received post-study therapy. All of these nine patients were past or current smokers, and six had emphysema at baseline (not detected prior to treatment, but diagnosed at the extramural review by a radiologist in the DSMC). Multivariate analyses were performed for the occurrence of ILD-like events using the logistic regression model and emphysema at baseline was indicated as a risk factor for onset of ILD-like events (odds ratio [95% CI], 12.13 [1.01–145.7]; P = 0.0491).

Adverse events led to erlotinib discontinuation in 30 patients (28.3%) and gemcitabine discontinuation in 27 patients (25.5%). The main reasons for treatment discontinuation were ILD (n = 6) and anorexia (n = 3); no patient discontinued treatment due to RASH or diarrhea. Due to the onset of AE, a total of 65 patients (61.3%) required one or more interruptions of erlotinib (36 patients [34.0%] for longer than seven consecutive days and 17 patients [16.0%] for longer than 14 consecutive days) and 56 patients (52.8%) had one or more skip of gemcitabine. Modifications in the erlotinib or gemcitabine dosage were required in 17 (16.0%) and 11 (10.4%) patients, respectively, due to AE.

Efficacy. The median OS was 9.23 months (95% CI, 8.31–10.78; Fig. 1A) and the 1-year survival rate was 33% (95% CI, 24–42). Median PFS was 3.48 months (95% CI, 2.63–3.78; Fig. 1B). Among the patients evaluable for tumor response (n = 64), the ORR was 20.3% (13/64; 95% CI, 11.3–32.2) and the DCR was 50.0% (95% CI, 37.2–62.8; CR, n = 0; PR, n = 13; stable disease, n = 19).

doi: 10.1111/j.1349-7006.2010.01810.x

Table 3. Characteristics, treatment and outcomes of patients with treatment-related ILD-like events (n = 9)

Event	Gender	Age (years)	Smoking status†	Days on treatment	ILD maximum grade	Suspicious findings of ILD	Steroids	Oxygen	ILD outcome	Presence of emphysema (assessed by radiologist)	Survival outcome (days)	Post-therapy (chemotherapy)
Lymphoid ILD	M	62	Past	82	1	Pyrexia	None	No	Improved	Yes	362	Yes
ILD	M	42	Current	50	3	Pyrexia	Pulse	Yes	Recovered	Yes	517	Yes
Organising pneumonia	M	60	Past	183	2	Respiratory symptoms	None	No	Improved	Yes	568+	Yes
ILD	F	62	Past	113	2	Cough	Oral	No	Recovered	Yes	376	No
ILD	F	74	Past	111	3	Cough, dyspnea	Pulse	Yes	Improved	None	183	No
ILD	M	60	Current	25	1	Pyrexia	Pulse	No	Recovered	None	119	Yes
ILD	M	77	Past	7	1	X-ray	None	No	Recovered	Yes	255	No
ILD	M	55	Past	187	1	CT	None	No	Recovered	Yes	415	No
ILD	F	60	Current	76	2	Cough	Oral	No	Recovered	None	346	Yes

†Past smoker, passage of at least 1 month since stopping smoking (at the time of registration); current smoker, smoked within 1 month (at the time of registration). CT, computed tomography; F, female; ILD, interstitial lung disease; M, male.

The median OS was longer in patients who experienced RASH of grade ≥2 (n = 67) than in those with RASH of grade ≤1 (n = 39) (10.25 months [95% CI, 8.80–12.12] *vs* 8.31 months [95% CI, 6.18–9.99], respectively; Fig. 1C) and the 1-year survival rate was higher (39% [95% CI, 27–50] *vs* 23% [95% CI, 10–36], respectively). Similarly, the median PFS was longer in patients with RASH of grade ≥2 versus those with RASH grade ≤1 (3.61 months [95% CI, 3.48–5.32] *vs* 1.81 months [95% CI, 1.64–3.48]; Fig. 1D). While there was no notable difference in ORR between patients with RASH grade ≥2 and those with grade ≤1 (21.1% [95% CI, 9.6–37.3] *vs* 19.2% [95% CI, 6.6–39.4]), the DCR was higher in those with more severe RASH (60.5% [95% CI, 43.4–76.0] *vs* 34.6% [95% CI, 17.2–55.7]).

Pharmacokinetics. Plasma sampling for PK analyses was performed in all six patients enrolled in the first step. On day 8, the values of C_{max} were 1760 ± 456.9 ng/mL (mean ± SD) for erlotinib, 169.7 ± 64.5 ng/mL for OSI-420 and 22 700 ± 3272.9 ng/mL for gemcitabine. The AUC_{last} was 29 001 ± 6560 h ng/mL, 2748 ± 788 h ng/mL and 10 717 ± 1458 h ng/mL (mean ± SD), respectively. The mean t_{max} was 8.0 h (range, 2.0–23.9 h), 9.0 h (2.0–23.9 h) and 0.51 h (0.45–0.57 h), respectively. Also on day 8, the mean plasma $t_{1/2}$ was 54.92 h (range, 9.25–144.61 h), 32.79 h (10.36–60.46 h), and 0.63 h (0.31–1.14 h), respectively. The Cl/F of erlotinib and gemcitabine showed interindividual variability; the Cl/F on day 8 was 3972.6 ± 772.1 mL/h (mean ± SD; coefficient of variation 19.4%) and 146 580.4 ± 31 101.3 mL/h (21.2%), respectively.

Biomarker analysis. Of the 106 patients enrolled, *EGFR* mutation status was evaluated in 47 patients (44.3%), all of whom had wild-type *EGFR*. The mutation status of the remaining patients was classified as unknown because samples were not available (30.2%), not examined (9.4%) or the results following sequencing were inconclusive (16.0%).

Discussion

This study was designed to initially assess the safety of erlotinib with gemcitabine for Japanese patients with pancreatic cancer, in whom there had been no prior exposure to either drug. As no significant safety concerns were raised in the first step of the study, enrollment of a further 101 patients was performed. Although the incidence of AE in this study was higher than in the PA.3 study, the incidence of grade 3–4 AE was similar.[28] Despite these results, no new AE specific to Japanese patients were observed. As expected, RASH and gastrointestinal events were among the most common AE in this study, and most of these cases were mild to moderate in severity.

Interstitial lung disease-like events were reported in nine patients (8.5%; grade 1/2/3, 3.8/2.8/1.9%) in the current study, while its incidence was reported to be 2.4% in patients treated in the erlotinib plus gemcitabine arm of the PA.3 study.[28] In addition, in Japanese patients with advanced pancreatic cancer, ILD-like events were reported in two (6.1%) of 33 patients treated with gemcitabine plus S-1, and were reported in three (1.1%) of 264 patients with gemcitabine monotherapy, respectively.[33,34] Likewise, the higher incidence of ILD-like events were documented using S-1 or erlotinib in combination with gemcitabine compared with gemcitabine as monotherapy in patients with pancreatic and biliary tract cancer.[35] On another front, outside of Japan, a high incidence of ILD-like events was reported in gemcitabine and paclitaxel combination therapy in patients with NSCLC.[36] From the above information, considering the higher incidence of ILD when gemcitabine is used in combination, an additive effect from such combinations cannot be ruled out.

In NSCLC, Japanese patients have an increased risk of developing ILD-like events when treated with EGFR TKI.[29,37–39] Fatal cases of ILD-like events have been reported following EGFR TKI administration for the treatment of NSCLC.[37–41] Importantly, however, no patients died due to an ILD-like event in this study. Seven patients experienced ILD-like events of grade 1–2 in severity. This may be due to active management of ILD-like cases during the study period. This management included regular and immediate chest X-rays, in addition to diagnosis with CT scans after any early signs and symptoms were observed (e.g. pyrexia, cough or dyspnea), timely discontinuation of the antitumor drugs (as a precautionary measure in case these drugs were associated with the symptoms) and appropriate treatment for the events (including oral/pulse steroids). By appropriately treating the early symptoms of ILD-like events, patients could restart antitumor therapy (chemotherapy: treatment change). In this study, the onset time for ILD-like events varied markedly between patients (7–187 days). It is therefore necessary to monitor the patients throughout the treatment period.

All of the patients who developed ILD in this study were current or past smokers, and smoking status has been shown to be a risk factor for ILD in the NSCLC population.[38] Results from the multivariate analyses in this study suggest that emphysema is also a risk factor for developing ILD; six of the nine

patients with ILD-like events were diagnosed with emphysema at baseline. Although the number of reports of an ILD-like event may have been artificially elevated due to underlying patient baseline characteristics and the active management of ILD-like events, these results demonstrate the need to consider the risk of ILD-like events in Japanese patients treated with TKI. In particular, it is important that chest CT scans are closely checked for the presence of emphysema or comorbid ILD and that pulmonary status is assessed prior to treatment administration.

This study corroborates the results of the combination of gemcitabine and erlotinib shown in the PA.3 study. The median OS in this study of 9.23 months was longer than those reported in trials with gemcitabine alone. In this study, patients who experienced skin toxicity of grade ≥2 had better outcomes than those with less severe toxicity or the overall study population. Retrospective analyses of data from the PA.3 and AViTA studies have found a significant association between the development of skin toxicity and efficacy in patients with pancreatic cancer treated with erlotinib-based therapy, although the precise mechanisms for the association between skin toxicity and effectiveness are unknown.[28,41,42]

Although the presence of mutations in the tyrosine-kinase region of the *EGFR* gene appears to predict a better response to erlotinib in NSCLC,[43,44] this has not yet been evaluated in pancreatic cancer. *EGFR* mutations are very rare in patients with pancreatic cancer;[45–47] indeed in the present study, no *EGFR* mutations were detected. Further work is required to determine whether *EGFR* mutations can be used as predictive markers for improved survival in Japanese patients receiving erlotinib and gemcitabine as treatment for advanced pancreatic cancer.

In conclusion, the present study shows that erlotinib in combination with gemcitabine is generally well tolerated in Japanese patients with advanced pancreatic cancer. This combination is associated with efficacy and survival outcomes, and the results of this study are consistent with the findings of the global PA.3 study.

Acknowledgments

The authors would like to thank all the patients, investigators and site staff involved in the study. We are grateful to Masahiro Fukuoka for acting as a medical advisor for this study. The authors also thank Abdul Al Khateeb of Gardiner–Caldwell Communications for editorial assistance. This study was sponsored by Chugai Pharmaceutical Co., Ltd. Editorial assistance from Abdul Al Khateeb of Gardiner–Caldwell Communications was funded by Chugai Pharmaceutical Co., Ltd.

Disclosure Statement

Junji Furuse received honoraria for lecture fees from Bayer, Eli Lilly Japan, Taiho Pharmaceutical and Eisai; Kazuhiko Nakagawa received honoraria for lecture fees from Eli Lilly Japan, Chugai Pharmaceutical and AstraZeneca; Takuji Okusaka, Akihiro Funakoshi, Tatsuya Ioka, Kenji Yamao, Shinichi Ohkawa, Narikazu Boku, Yoshito Komatsu, Shoji Nakamori, Haruo Iguchi, Tetsuhide Ito and Kohei Nakachi have no conflict of interest.

References

1 Parkin DM, Bray F, Ferlay J *et al.* Global cancer statistics, 2002. *CA Cancer J Clin* 2005; **55**: 74–108.
2 Japanese Ministry of Health, Labour and Welfare. Statistical investigation result 2005. (In Japanese.) [Cited 16 Feb 2010.] Available from URL: http://www-bm.mhlw.go.jp/toukei/saikin/hw/kanja/05syoubyo/index.html.
3 Japanese Ministry of Health, Labour and Welfare. Table database system. (In Japanese.) [Cited 16 Feb 2010.] Available from URL: http://www.mhlw.go.jp/toukei/youran/indexyk_1_2.html.
4 Burris HA III, Moore MJ, Andersen J *et al.* Improvements in survival and clinical benefit with gemcitabine as first-line therapy for patients with advanced pancreas cancer: a randomized trial. *J Clin Oncol* 1997; **15**: 2403–13.
5 Berlin JD, Catalano P, Thomas JP *et al.* Phase III study of gemcitabine in combination with fluorouracil versus gemcitabine alone in patients with advanced pancreatic carcinoma: Eastern Cooperative Oncology Group Trial E2297. *J Clin Oncol* 2002; **20**: 3270–5.
6 Colucci G, Giuliani F, Gebbia V *et al.* Gemcitabine alone or with cisplatin for the treatment of patients with locally advanced and/or metastatic pancreatic carcinoma: a prospective, randomized phase III study of the Gruppo Oncologia dell'Italia Meridionale. *Cancer* 2002; **94**: 902–10.
7 Rocha Lima CM, Green MR, Rotche R *et al.* Irinotecan plus gemcitabine results in no survival advantage compared with gemcitabine monotherapy in patients with locally advanced or metastatic pancreatic cancer despite increased tumor response rate. *J Clin Oncol* 2004; **22**: 3776–83.
8 Louvet C, Labianca R, Hammel P *et al.* Gemcitabine in combination with oxaliplatin compared with gemcitabine alone in locally advanced or metastatic pancreatic cancer: results of a GERCOR and GISCAD phase III trial. *J Clin Oncol* 2005; **23**: 3509–16.
9 Oettle H, Richards D, Ramanathan RK *et al.* A phase III trial of pemetrexed plus gemcitabine versus gemcitabine in patients with unresectable or metastatic pancreatic cancer. *Ann Oncol* 2005; **16**: 1639–45.
10 Abou-Alfa GK, Letourneau R, Harker G *et al.* Randomized phase III study of exatecan and gemcitabine compared with gemcitabine alone in untreated advanced pancreatic cancer. *J Clin Oncol* 2006; **24**: 4441–7.
11 Heinemann V, Quietzsch D, Gieseler F *et al.* Randomized phase III trial of gemcitabine plus cisplatin compared with gemcitabine alone in advanced pancreatic cancer. *J Clin Oncol* 2006; **24**: 3946–52.
12 Stathopoulos GP, Syrigos K, Aravantinos G *et al.* A multicenter phase III trial comparing irinotecan-gemcitabine (IG) with gemcitabine (G) monotherapy as first-line treatment in patients with locally advanced or metastatic pancreatic cancer. *Br J Cancer* 2006; **95**: 587–92.
13 Herrmann R, Bodoky G, Ruhstaller T *et al.* Gemcitabine plus capecitabine compared with gemcitabine alone in advanced pancreatic cancer: a randomized, multicenter, phase III trial of the Swiss Group for Clinical Cancer Research and the Central European Cooperative Oncology Group. *J Clin Oncol* 2007; **25**: 2212–7.
14 Van Cutsem E, van de Velde H, Karasek P *et al.* Phase III trial of gemcitabine plus tipifarnib compared with gemcitabine plus placebo in advanced pancreatic cancer. *J Clin Oncol* 2004; **22**: 1430–8.
15 Bramhall SR, Rosemurgy A, Brown PD *et al.* Marimastat as first-line therapy for patients with unresectable pancreatic cancer: a randomized trial. *J Clin Oncol* 2001; **19**: 3447–55.
16 Moore M, Hamm J, Dancey J *et al.* Comparison of gemcitabine versus the matrix metalloproteinase inhibitor BAY 12-9566 in patients with advanced or metastatic adenocarcinoma of the pancreas: a phase III trial of the National Cancer Institute of Canada Clinical Trials Group. *J Clin Oncol* 2003; **21**: 3296–302.
17 Philip PA, Benedetti J, Fenoglio-Preiser C *et al.* Phase III study of gemcitabine [G] plus cetuximab [C] versus gemcitabine in patients [pts] with locally advanced or metastatic pancreatic adenocarcinoma [Pca]: SWOG S0205 study. *J Clin Oncol* 2007; **25** (Suppl 18): 199s (Abstract LBA4509).
18 Kindler HL, Niedzwiecki D, Hollis E *et al.* A double-blind, placebo-controlled, randomizes phase III trial of gemcitabine (G) plus bevacizumab (B) versus gemcitabine plus placebo (P) in patients (pts) with advanced pancreatic cancer (PC): A Preliminary Analysis of Cancer and Leukemia Group B (CALGB). *J Clin Oncol* 2007; **25** (Suppl 18): 199s (Abstract 4508).
19 Van Cutsem E, Vervenne WL, Bennouna J *et al.* Phase III trial of bevacizumab in combination with gemcitabine and erlotinib in patients with metastatic pancreatic cancer. *J Clin Oncol* 2009; **27**: 2231–7.
20 Lynch TJ Jr, Kim ES, Eaby B *et al.* Epidermal growth factor receptor inhibitor-associated cutaneous toxicities: an evolving paradigm in clinical management. *Oncologist* 2007; **12**: 610–21.
21 Perez-Soler R, Saltz L. Cutaneous adverse effects with HER1/EGFR-targeted agents: is there a silver lining? *J Clin Oncol* 2005; **23**: 5235–46.
22 Arteaga C. Targeting HER1/EGFR: a molecular approach to cancer therapy. *Semin Oncol* 2003; **30**: 3–14.
23 Harari D, Yarden Y. Molecular mechanisms underlying ErbB2/HER2 action in breast cancer. *Oncogene* 2000; **19**: 6102–14.
24 Jost M, Gasparro FP, Jensen PJ *et al.* Keratinocyte apoptosis induced by ultraviolet B radiation and CD95 ligation – differential protection through epidermal growth factor receptor activation and Bcl-x(L) expression. *J Invest Dermatol* 2001; **116**: 860–6.
25 Quon H, Liu F, Cummings B. Potential molecular prognostic markers in head and neck squamous cell carcinomas. *Head Neck* 2001; **23**: 147–59.

doi: 10.1111/j.1349-7006.2010.01810.x

26 Ueda S, Ogata S, Tsuda H *et al.* The correlation between cytoplasmic overexpression of epidermal growth factor receptor and tumor aggressiveness: poor prognosis in patients with pancreatic ductal adenocarcinoma. *Pancreas* 2004; **29**: e1–8.
27 Durkin A, Bloomston PM, Rosemurgy AS *et al.* Defining the role of the epidermal growth factor receptor in pancreatic cancer grown *in vitro*. *Am J Surg* 2003; **186**: 431–6.
28 Moore M, Goldstein D, Hamm J *et al.* Erlotinib plus gemcitabine compared with gemcitabine alone in patients with advanced pancreatic cancer: a phase III trial of the National Cancer Institute of Canada Clinical Trials Group. *J Clin Oncol* 2007; **25**: 1960–6.
29 Kubota K, Nishiwaki Y, Tamura T *et al.* Efficacy and safety of erlotinib monotherapy for Japanese patients with advanced non-small cell lung cancer: a phase II study. *J Thorac Oncol* 2008; **3**: 1439–45.
30 Dragovich T, Huberman M, Von Hoff DD *et al.* Erlotinib plus gemcitabine in patients with unresectable pancreatic cancer and other solid tumors: phase IB trial. *Cancer Chemother Pharmacol* 2007; **60**: 295–303.
31 Honeywell R, Laan AC, van Groeningen CJ *et al.* The determination of gemcitabine and 2′-deoxycytidine in human plasma and tissue by APCI tandem mass spectrometry. *J Chromatogr B Analyt Technol Biomed Life Sci* 2007; **847**: 142–52.
32 Ling J, Fettner S, Lum BL *et al.* Effect of food on the pharmacokinetics of erlotinib, an orally active epidermal growth factor receptor tyrosine-kinase inhibitor, in healthy individuals. *Anticancer Drugs* 2008; **19**: 209–16.
33 Nakamura K, Yamaguchi T, Ishihara T *et al.* Phase II trial of oral S-1 combined with gemcitabine in metastatic pancreatic cancer. *Br J Cancer* 2006; **94**: 1575–9.
34 Tanaka T, Ikeda M, Okusaka T *et al.* Prognostic factors in Japanese patients with advanced pancreatic cancer treated with single-agent gemcitabine as first-line therapy. *Jpn J Clin Oncol* 2008; **38**: 755–61.
35 Tamiya A, Endo M, Shukuya T *et al.* Features of gemcitabine-related severe pulmonary toxicity patients with pancreatic or biliary tract cancer. *Pancreas* 2009; **38**: 838–40.
36 Bhatia S, Hanna N, Ansari R *et al.* A phase II study of weekly gemcitabine and paclitaxel in patients with previously untreated stage IIIb and IV non-small cell lung cancer. *Lung Cancer* 2002; **38**: 73–7.
37 Ando M, Okamoto I, Yamamoto N *et al.* Predictive factors for interstitial lung disease, antitumor response, and survival in non-small-cell lung cancer patients treated with gefitinib. *J Clin Oncol* 2006; **24**: 2549–56.
38 Kudoh S, Kato H, Nishiwaki N *et al.* Interstitial lung disease in Japanese patients with lung cancer: a cohort and nested case–control study. *Am J Respir Crit Care Med* 2008; **177**: 1348–57.
39 Tsuboi M, Le Chevalier T. Interstitial lung disease in patients with non-small-cell lung cancer treated with epidermal growth factor receptor inhibitors. *Med Oncol* 2006; **23**: 161–70.
40 Yoneda KY, Shelton DK, Beckett LA *et al.* Independent review of interstitial lung disease associated with death in TRIBUTE (paclitaxel and carboplatin with or without concurrent erlotinib) in advanced non-small cell lung cancer. *J Thorac Oncol* 2007; **2**: 537–43.
41 Wacker B, Nagrani T, Weinberg J *et al.* Correlation between development of rash and efficacy in patients treated with the epidermal growth factor receptor tyrosine kinase inhibitor erlotinib in two large phase III studies. *Clin Cancer Res* 2007; **13**: 3913–21.
42 Van Cutsem E, Vervenne WL, Bennouna J *et al.* Rash as a marker for the efficacy of gemcitabine plus erlotinib-based therapy in pancreatic cancer: results from the AViTA study. Proc ASCO Gastrointestinal Cancers Symposium, 2009 (Abstr 117). [Cited 16 Feb 2010.] Available from URL: http://www.asco.org/ASCOv2/Meetings/Abstracts?&vmview=abst_detail_view&confID=63&abstractID=10514.
43 Tsao MS, Sakurada A, Cutz JC *et al.* Erlotinib in lung cancer – molecular and clinical predictors of outcome. *N Engl J Med* 2005; **353**: 133–44.
44 Zhu CQ, da Cunha Santos G, Ding K *et al.* Role of KRAS and EGFR as biomarkers of response to erlotinib in National Cancer Institute of Canada Clinical Trials Group Study BR.21. *J Clin Oncol* 2008; **28**: 4268–75.
45 Immervoll H, Hoem D, Kugarajh K *et al.* Molecular analysis of the EGFR-RAS-RAF pathway in pancreatic ductal adenocarcinomas: lack of mutations in the BRAF and EGFR genes. *Virchows Arch* 2006; **448**: 788–96.
46 Lee J, Jang KT, Ki CS *et al.* Impact of epidermal growth factor receptor (EGFR) kinase mutations, EGFR gene amplifications, and KRAS mutations on survival of pancreatic adenocarcinoma. *Cancer* 2007; **109**: 1561–9.
47 Tzeng CW, Frolov A, Frolova N *et al.* Epidermal growth factor receptor (EGFR) is highly conserved in pancreatic cancer. *Surgery* 2007; **141**: 464–9.

Clin Exp Metastasis (2011) 28:13–25
DOI 10.1007/s10585-010-9354-8

RESEARCH PAPER

Interaction between lung cancer cells and astrocytes via specific inflammatory cytokines in the microenvironment of brain metastasis

Toshihiro Seike · Kyota Fujita · Yukiko Yamakawa · Mizuho A. Kido · Soichi Takiguchi · Norihiro Teramoto · Haruo Iguchi · Mami Noda

Received: 13 July 2009 / Accepted: 25 September 2010 / Published online: 17 October 2010

Abstract The incidence of brain metastasis is increasing, however, little is known about molecular mechanism responsible for lung cancer-derived brain metastasis and their development in the brain. In the present study, brain pathology was examined in an experimental model system of brain metastasis as well as in human brain with lung cancer metastasis. In an experimental model, after 3–6 weeks of intracardiac inoculation of human lung cancer-derived (HARA-B) cells in nude mice, wide range of brain metastases were observed. The brain sections showed significant increase in glial fibrillary acidic protein (GFAP)-positive astrocytes around metastatic lesions. To elucidate the role of astrocytes in lung cancer proliferation, the interaction between primary cultured mouse astrocytes and HARA-B cells was analyzed in vitro. Co-cultures and insert-cultures demonstrated that astrocytes were activated by tumor cell-oriented factors; macrophage migration inhibitory factor (MIF), interleukin-8 (IL-8) and plasminogen activator inhibitor-1 (PAI-1). Activated astrocytes produced interleukin-6 (IL-6), tumor necrosis factor-α (TNF-α) and interleukin-1 β (IL-1β), which in turn promoted tumor cell proliferation. Semi-quantitative immunocytochemistry showed that increased expression of receptors for IL-6 and its subunits gp130 on HARA-B cells. Receptors for TNF-α and IL-1β were also detected on HARA-B cells but down-regulated after co-culture with astrocytes. Insert-culture with astrocytes also stimulated the proliferation of other lung cancer-derived cell lines (PC-9, QG56, and EBC-1). These results suggest that tumor cells and astrocytes stimulate each other and these mutual relationships may be important to understand how lung cancer cells metastasize and develop in the brain.

Keywords Interleukin-8 · Macrophage migration inhibitory factor · Plasminogen activator inhibitor-1 · Interleukin-6 · Tumor necrosis factor-α · Interleukin-1β

The study was approved by the Animal Care and Use Committee at Kyushu University and carried out in accordance with the National Institutes of Health Guide for the Care and Use of Laboratory Animals.

Electronic supplementary material The online version of this article (doi:10.1007/s10585-010-9354-8) contains supplementary material, which is available to authorized users.

T. Seike · K. Fujita · Y. Yamakawa · M. Noda (✉)
Laboratory of Pathophysiology, Graduate School of Pharmaceutical Sciences, Kyushu University, 3-1-1 Maidashi, Higashi-ku, Fukuoka 812-8582, Japan
e-mail: noda@phar.kyushu-u.ac.jp

M. A. Kido
Department of Oral Anatomy and Cell Biology, Graduate School of Dental Sciences, Kyushu University, Fukuoka 812-8582, Japan

S. Takiguchi
Institute for Clinical Research, National Kyushu Cancer Center, Fukuoka 811-1395, Japan

N. Teramoto
Division of Pathology, National Hospital Organization Shikoku Cancer Center, Matsuyama, Ehime 791-0280, Japan

H. Iguchi
Clinical Research Institute, National Hospital Organization Shikoku Cancer Center, Matsuyama, Ehime 791-0280, Japan

Abbreviations

ab	Antibody
ACM	Astrocyte conditioned medium
BSA	Bovine serum albumin
Cdna	Complementary DNA

DAPI	4′,6′-diamidino-2-phenylindole hydrochloride
DMEM	Dulbecco's modified Eagle medium
EDTA	Ethylenediaminetetraacetic acid
EGFR	Epidermal growth factor receptor
FCS	Fetal calf serum
FITC	Fluoresceinisothiocyanate
GFAP	Glial fibrillary acidic protein
MT1-MMP	Membrane type-1 matrix metalloproteinase
HCM	HARA-B conditioned medium
H-ACM	HARA-B-astrocytes conditioned medium
ICM	Insert culture medium
IGF-1	Insulin-like growth factor-1
IL-1β	Interleukin-1β
IL-1ra	Interleukin-1 receptor antagonist
IL-3	Interleukin-3
IL-6	Interleukin-6
MIF	Macrophage migration inhibitory factor
PAI-1	Plasminogen activator inhibitor
PBS	Phosphate buffer saline
PDGF	Platelet-derived growth factor
PFA	Paraformaldehyde
PTHrP	Parathyroid hormone-related protein
SERPINE1	Serpin peptidase inhibitor plasminogen activator inhibitor type 1)
TGF-β	Transforming growth factor-β
TNF-α	Tumor necrosis factor-α

Introduction

Metastasis is the principal cause of the morbidity and death of cancer patients. The incidence of brain metastasis has been increasing in recent years, especially in breast cancer and lung cancer [1]. In the process of metastasis formation, the interaction between the metastatic tumor cells and host cells plays an important role in the microenvironment of the metastatic sites [2]. However, a molecular mechanism for brain metastasis is poorly understood to date. In the central nervous system, activated glial cells contribute to the innate immune response and produce a large variety of different inflammatory mediators as a chronic inflammatory reaction [3]. A similar mechanism could function in cell survival, growth, proliferation and colonization, invasion and motility of metastatic tumor cells in the microenvironment of brain metastases [4, 5]. Among the glial cells, astrocytes are the most abundant cell population and play an important role in maintaining homeostasis of the brain [6]. Astrocytes have been shown to produce a wide variety of cytokines including interleukin-1 (IL-1), interleukin-3 (IL-3), interleukin-6 (IL-6), tumor necrosis factor-α (TNF-α), transforming growth factor-β (TGF-β), insulin-like growth factor-1 (IGF-1) and platelet-derived growth factor (PDGF) [7–10]. Among them, it was suggested that IL-6, TGF-β and IGF-1 may contribute to the development of brain metastasis by breast cancer cells [11]. As for brain metastasis by lung cancer cells, it is not known whether or not the same cytokines are involved and what the difference between brain metastases derived by breast cancer cells and lung cancer cells.

Therefore, in the present study, we examined brain pathology in an experimental model system of brain metastasis, using HARA-B cells derived from human lung cancer cells, and assessed the effects of astrocytes on the growth of HARA-B cells as well as three other non-small cell lung cancer cell lines (PC-9, QG56, and EBC-1) in vitro. Furthermore, astrocytes-derived factors conducive to tumor cell growth and their receptor expression on tumor cells were investigated.

Materials and methods

Experimental model for brain metastasis

The study was approved by the Animal Care and Use Committee at Kyushu University and carried out in accordance with the National Institutes of Health Guide for the Care and Use of Laboratory Animals. Male 5-week-old nude mice (BALB/c *nu/nu*) (Kyudo, Kumamoto, Japan), kept in a specific pathogen-free environment, were used. A single suspension of human lung squamous cell carcinoma-derived cells (HARA-B) (2×10^5 cells/0.2 ml PBS) was inoculated into the left ventricle of the heart in nude mice according to the method described previously [12]. After 4–6 weeks, brains were subjected for immunohistochemical staining.

Human tissue samples

A total of 6 paraffin-embedded samples from patients with lung tumor brain metastasis were used. All sections were obtained from the National Hospital Organization Shikoku Cancer Center. Use of the human specimens was in accordance with the University Ethics Commission. The formalin-fixed, paraffin-embedded archival tissue blocks were retrieved, and matching hematoxylin and eosin (H & E)-stained slides were reviewed and screened for representative tumor regions by a neuropathologist.

Immunohistochemistry

Nude mice were perfused transcardially with 50 ml of 10 U/ml heparin and 0.5% procaine in PBS and 4% paraformaldehyde (PFA) in PBS prior to excision of the brain.

Then the brain was removed, post-fixed for 3 h, and cryoprotected for 24 h in PBS containing 20% sucrose. The brain was cut into slices (30 μm thick) using a cryostat and the sections were placed on glass slides. In order to acquire the better immunoreactive images, sections were autoclaved with 0.01 M citrate buffer solution (pH 6.0), permeabilized with 0.3% TritonX-100 in PBS for 15 min, and then blocked in BlockAce (Dainippon Pharmaceutical, Japan) for 1 h at room temperature. Sections were incubated with mouse anti-human cytokeratin monoclonal antibody (AE1/AE3 pool of cytokeratin) (Dako, Glostrup, Denmark, 1:100) at 4°C overnight. Biotinylated anti-mouse IgG (Jackson, 1:200) were incubated for 2 h at room temperature, followed by the incubation with streptavidin Alexa488 (Molecular Probes, 1:500) for 2 h at room temperature. For double-staining of cytokeratin and GFAP, sections were incubated with Cy3-conjugated anti-GFAP antibody (Sigma, USA) (1:1000) at 4°C overnight after staining of cytokeratin. Every treatment was followed by washing three times with PBS containing 0.3% TritonX-100 for 5 min. The sections were mounted in the Perma Fluor Aqueous Mounting Medium (Thermo Shandon, Pittsburgh, PA, USA) and analyzed with a confocal microscope (LSM510 META, Carl Zeiss, Co. Ltd. Germany). Z-stack images were obtained from each section by LSM 510 META and total intensity were calculated by LSM image browser.

As for human tissue samples, after removal of paraffin in xylene and rehydration in a graded of alcohols (100%, 90%, 80%, 70%, 60%), sections were incubated for 30 min in 0.05 M phosphate buffer pH 7.6 containing tripsin and KCl for antigen retrieval. Then, the sections were incubated for 1 h in 0.3% H_2O_2, and blocked in PBS containing 1% BSA and 5% normal donkey serum (Jackson Immuno Research Laboratories Inc., West Grove, PA, USA) for 1 h at room temperature. Then, the sections were incubated with anti-GFAP antibody (ImmunoStar) (1:15) at 4°C overnight, goat anti-rabbit IgG Alexa 568 (Molecular Probes) (1:500) for 3 h at room temperature and FITC-conjugated anti-human cytokeratin antibody (CAM5.2) (Becton–Dickinson Biosciences, New Jersey, USA) (undiluted solution) for 1 h at room temperature. Every treatment was followed by washing three times with PBS containing 0.3% TritonX-100 for 5 min. The sections were mounted in the Perma Fluor Aqueous Mounting Medium (Thermo Shandon, Pittsburgh, PA, USA) and analyzed with a confocal microscope (LSM510 META, Carl Zeiss, Co. Ltd. Germany).

Cell culture

Primary glial cell cultures were performed according to the method described previously [13]. Briefly, the cerebral cortex obtained from 1-day-old C57BL/6 mice (Kyudo, Kumamoto, Japan) were isolated under a dissecting microscope and carefully separated from the choroid plexus and meninges. The isolated cerebral cortex were minced and treated with trypsin–EDTA solution (0.25% trypsin, 1 mM EDTA) and 1500 U DNase in Dulbecco's modified Egle medium (DMEM; Nissui, Tokyo, Japan) at 37°C for 10 min. Cell suspensions were filtered through 70 μm pore size mesh (BD Falcon, Bedford, MA, USA) into DMEM containing 10% fetal calf serum (FCS; Hyclone, UT, USA), 2 mM L-glutamine, 100 U/ml penicillin, 100 μg/ml streptomycin, 0.37% $NaHCO_3$, and 110 μg/ml pyruvic acid. After centrifugation, cells were filtered through 40 μm pore size-mesh (BD Falcon), plated into poly-L-lysine coated 75 cm^2 cell culture flask at the density of two brains per flask in 10 ml of DMEM, and maintained at 37°C in 10% CO_2–90% air with a change of the medium twice per week. Astrocytes were obtained after 28 days of mixed glial cell cultures as follows. After removing other glial cells by shaking the flasks, the astroglial layer was removed from the flasks by the treatment with trypsin–EDTA solution (0.06% trypsin, 0.25 mM EDTA in serum free DMEM) at 37°C for 45 min. Suspended astrocytes were filtered through 40 μm pore size-mesh and seeded. Astrocyte purity ranged from 90 to 95% as determined by immunostaining with anti-GFAP antibody (Sigma, St. Louis, MO, USA) (data not shown). Astrocytes were maintained in the same medium used for cell suspension from cerebral cortex at 37°C in 10% CO_2–90% air. HARA-B cells and other lung cancer cell lines (QG56, EBC-1; squamous cell carcinoma) and PC-9 (non-small cell lung cancer cell) were maintained under the same condition. Cells were grown in 25 cm^2 cell culture flask (Nalge Nunc International), and single-cell suspension of cells were obtained by trypsin treatment.

Cell proliferation assay

In the co-culture experiment, HARA-B cells (0.5×10^3 cells/well) and astrocytes (2.5×10^3 or 5×10^3 cells/well) were seeded into 8-well cell culture slide (BD Falcon) in DMEM for 24 h. Then, cells were rinsed twice with PBS and incubated in serum free DMEM. After 72 h of co-culture, cells were fixed with 4% PFA for 30 min at room temperature and permeabilized with 0.3% TritonX-100 in PBS for 15 min, followed with blocking solution containing 1% BSA and 5% normal donkey serum (Jackson) in PBS for 1 h at room temperature. Then cells were incubated with mouse anti-human cytokeratin monoclonal antibody (AE1/AE3 pool of cytokeratin) (Dako, Glostrup, Denmark) (1:100) at 4°C overnight, followed by the incubation with the secondary antibody (FITC-conjugated anti-mouse IgG; Sigma, 1:500) for 5 h at room temperature, and then, incubated with 300 nM 4′,6′-diamidino-2-phenylindole hydrochloride (DAPI, Sigma) for 30 min at

room temperature. The number of HARA-B cells in each well, which were positively stained with an anti-human cytokeratin antibody, was counted using a digital camera system (Axio Cam, Carl Zeiss) mounted on a light and fluorescent microscope (Axopscope2 plus, Carl Zeiss). The results were expressed as the percentage of control (single cell culture of HARA-B cells).

Insert culture-medium was obtained as follows. Astrocytes (5×10^4 cells/well) were plated in 6-well cell culture plates (Falcon). Tumor cells derived from each lung tumor (EBC-1, PC9, QG56 and HARA-B cells) (5×10^3 cells/insert) were plated in cell culture-inserts (membrane pore size 0.4 μm; Becton–Dickinson), and then, placed in the well of astrocyte cultures. After 24 h of the insert-culture, cells were rinsed twice with PBS, incubated in serum-free DMEM for further 48 h. Then, the medium was collected. Each conditioned medium was centrifuged to remove debris (1500 rpm for 10 min at 4°C) before use. Tumor cells derived from each lung tumor (0.5×10^3 cells/well) were seeded into 8-well cell culture slide (BD Falcon) in DMEM for 24 h. Then, cells were rinsed twice with PBS and incubated in each Insert culture-medium. After 72 h, cells were fixed with 4% PFA for 30 min at room temperature and incubated with 300 nM DAPI for 10 min at room temperature. The number of tumor cells in each well, which were positively stained with DAPI, was counted as mentioned above. The results were expressed as the percentage of control (each tumor cells cultured in serum-free DMEM for 72 h).

The astrocyte-conditioned medium (ACM) was obtained from the primary culture of astrocytes at a density of 10^4 cells/well in serum free DMEM after 72 h-incubation. This ACM was centrifuged (1500 rpm for 10 min at 4°C), and then, added to HARA-B cells cultured for 1 day at a volume of 25% or 50%. The number of HARA-B cells were counted after the 72 h-incubation in the presence of ACM as described above.

HARA-B-stimulated astrocyte-conditioned medium (H-ACM) was obtained as follows. Culture medium of HARA-B cells (5×10^3 cells/well) were added to astrocytes cultures (5×10^4 cells/well) and incubated for 24 h. Then the medium was collected and centrifuged to remove debris (1500 rpm for 10 min at 4°C) before use.

In the proliferation assay using recombinant mouse cytokines, HARA-B cells 24 h after plating were rinsed twice with PBS and incubated in serum free DMEM with each cytokine (mIL-1β, 1 to 10 pg/ml; mTNF-α, 10 to 500 pg/ml; mIL-6, 10 to 500 pg/ml, Peprotech, Rocky Hill, NJ, USA). After 72 h, HARA-B cells were immunostained and counted as mentioned above.

In the experiments using neutralizing antibodies, cells were plated, rinsed twice with PBS after 24 h, and incubated in serum free DMEM with each specific neutralizing antibodies; mIL-1β antibody (ab), 0.2 to 2.0 μg/ml (R&D systems, Minneapolis, MN USA), mTNF-α ab, 0.2 to 2.0 μg/ml (R&D systems), mIL-6 ab, 2.0 to 20 ng/ml (Peprotech) for 48 h. As controls, rat IgG (Sigma) and rabbit IgG (R&D systems) were used. HARA-B cells were immunostained and counted as mentioned above.

SYBR green-based real-time quantitative RT–PCR

HARA-B cells (1×10^5 cells/insert) and astrocytes (1×10^6 cells/well) were cultured in cell culture-insert systems as mentioned above. Cells were collected by treatment with trypsin after 24, 48 and 72 h of insert-culture. As controls, single cell culture of HARA-B cells or astrocytes was used. Total RNA was isolated from each cell type by an extraction procedure using the RNA blood mini kit (QIAGEN in Japan). Contaminating DNA was removed by RNase-free DNase (QIAGEN). Single-strand cDNA was synthesized from cellular mRNA by using random 9 mer and RNA PCR kit (AMV) (Takara Bio Inc., Ootsu, Japan). PCR amplification was undertaken for plain SYBR Green I detection in using Light Cycler system (Roche Diagnostics GmbH, Mannheim, Germany). Each reaction was carried out in a total volume of 20 μl in glass capillary, containing 1 μl of cDNA, 2, 3 or 4 mM $MgCl_2$, 10% LightCycler-DNA Master SYBR Green I buffer (Taq DNA polymerase, reaction buffer, deoxynucleotide triphosphate mix, 10 mM $MgCl_2$ and SYBR Green I dye) and 0.5 μM of each primer (Table 1). After the PCR reaction, we confirmed that there was no primer dimer and non specific product in each PCR product by agarose gel electrophoresis and staining with ethidium bromide. The expression of all target genes was normalized to β-actin. Analysis was carried out with Light Cycler 3.5 software (Roche) and Microsoft Excel.

To see the reconstituted effects of HARA-B-derived substances on astrocytic expression of TNF-α, IL-1β and IL-6, the mouse primary astrocyte cells were treated with human IL-8 (R&D systems, Minneapolis, MN, U.S.A), MIF (R&D systems), or PAI-1 (Peprotech, Rocky Hill, U.S.A) for 72 h in serum-free medium. Total RNA was extracted using an RNeasy Plus Mini kit (QIAGEN, Hilden, Germany) and QIA shredder (QIAGEN). cDNA was synthesized using a SuperScript VILO cDNA synthesis kit (Invitrogen) SYBR-Green real-time PCR (Applied Biosystems, Foster City, CA) was performed on cDNA prepared from each sample using Platinum SYBR-Green qPCR Super-Mix-UDG (Invitrogen) and 0.5 μM each primer (Table 1). Thermal cycling condition were 10 min at 95°C, 45 cycles at 95°C for 15 s, followed by 1 min at 60°C. Data Analysis was completed using the ABI PRISM 7500HT Sequence detection software (Applied Biosystems). β-actin was used for normalization.

Table 1 Gene-specific primer pairs for real-time RT–PCR

	Primer sequence (5′–3′)		Length (bp)
Mouse			
β-actin	Sense	ACCAACTGGGACGACATGGAG	380
	Antisense	GTGGTG GTGAAG CTGTAGCC	
IL-6	Sense	ACAAGTCGGAGGCTTAATTACACAT	79
	Antisense	AATCAG AATTG CCATTGCACAA	
IL-1β	Sense	CTCCATGAG CTTTGTACAAG G	240
	Antisense	TG CTG ATGTACCAGTTG GG G	
TNF-α	Sense	ATGAGCACAGAAAGCATGATCCGC	692
	Antisense	CCAAAGTAGACCTG CCCG GACTC	
TGF-β1	Sense	GAG AG CCCTGG GATACCAACTACTG	173
	Antisense	GTGTGTCCAGG CTCCAAATGTAG	
EGF	Sense	TTTTGCCTCAGAAG GAGTGG	150
	Antisense	GG CCACACTTG G CAGTATATC	
IGF-I	Sense	GGACCAGAGACCCTTTGCGGGG	209
	Antisense	GG CTG CTTTTGTAGG CTTCAGTG G	
PDGF-B	Sense	TGAAATGCTGAGCGACCAC	137
	Antisense	AGCTTTCCAACTCGACTCC	
Human			
β-actin	Sense	ATG GCCACG GCTGCTTCCAG C	237
	Antisense	CATGGTGGTGACAGACCG CCG	
IL-6Ra	Sense	CATTGCCATTGTTCTGAGGTT	271
	Antisense	AGTAGTCTGTATTG CTGATGT	
gpi30	Sense	TGGAGTGAAGAAGCAAGTGG	303
	Antisense	AACAGCTGCATCTGATTTGC	
TNFRI	Sense	TG CCTACCCCAGATTG AG AA	121
	Antisense	ATTTCCCACAAACAATGGAGTAG	
IL-1 Rtl	Sense	AAG GTG GAG G ATTCAGG ACAT	284
	Antisense	AG CCTATCTTTGACTCCACTA	
IL-1 ra	Sense	CAGAAGACCTCCTGTCCTATGAGG	424
	Antisense	GCTGTGCAGAGGAACCA	

Cytokine ELISA assay

Co-cultures of HARA-B cells (0.5×10^3 cells/well) and astrocytes (5×10^3 cells/well) or astrocytes alone (5×10^3 cells/well) were seeded into 8-well cell culture slides in DMEM with FCS for 24 h. Then, cells were rinsed twice with PBS and incubated in serum free DMEM. After 48 or 72 h of culture, each conditioned medium was collected and centrifuged to remove debris (1500 rpm for 10 min at 4°C) before use. The amount of mouse IL-1β, TNF-α and IL-6 in each conditioned medium was measured with an ELISA kit for mouse cytokines (Biosource International). The absorbency at 450 nm was measured by a Microplate Reader (Immuno-Mini NJ-2300, Nalge Nunc International).

Cytokine proteome array

HARA-B cells (1×10^6 cells) were grown in 10 cm dish (BD, Franklin Lake, NJ, U.S.A) for 24 h and culture medium was collected. Protein array analysis was performed according to the manufacture's instruction. Positive controls were located in the upper left-hand corner (two spots), upper right-hand corner (two spots) and the lower left-hand corner (two spots) of each array kit. Medium and culture medium were measured using the human cytokine array Panel A (Proteome Profiler) (R&D systems, Minneapolis, MN, U.S.A). Horseradish peroxidase substrate (Thermo scientific, Rockford, IL, U.S.A) was used to detect protein expression and captured by exposure to X-ray Film (FUJIFILM, Tokyo, Japan).

Immunocytochemistry

HARA-B cells (0.5×10^3 cells/well) with or without astrocytes (5×10^3 cells/well) were seeded into 8-well cell culture slides in complete medium. Cells were fixed with 4% PFA for 30 min at room temperature and permeabilized with 0.3% TritonX-100 in PBS for 15 min and blocked

in PBS containing 1% BSA and 5% normal donkey serum (Jackson) for 1 h at room temperature. Cells were incubated with primary antibodies, containing monoclonal mouse anti-human cytokeratin antibody (AE1/AE3 pool of cytokeratin) (Dako, 1:100), rabbit anti-human IL-6Rα antibody (Santa Cruz, CA, USA) (1:200), rabbit anti-human gp130 antibody (Santa Cruz, 1:500), rabbit anti-human IL-1RtI antibody (Santa Cruz, 1:200), and goat anti-human TNFRI (Santa Cruz, 1:100) overnight at 4°C. Control cells were incubated without primary antibody (PBS containing 1% BSA) to test non-specific staining. The cells were then incubated for 5 h at room temperature with secondary antibody, containing FITC-conjugated anti-mouse IgG (Sigma, 1:500), Cy3-conjugated anti-rabbit IgG (Jackson, 1:500) and Cy3-conjugated anti-goat IgG (Jackson, 1:500) and then for 30 min at room temperature with 300 nM 4′,6′-diamidino-2-phenylindole hydrochloride (DAPI, Sigma). Slides were mounted in the Perma Fluor Aqueous Mounting Medium (Thermo) and were analyzed with a Zeiss LSM510 META confocal microscope.

Statistical analysis

One-way analysis of variance (ANOVA) and post-hoc Bonferroni/Dunn test were used to examine the statistical differences. Differences were considered significant at $P < 0.05$.

Results

Histological analyses of lung cancer cell-induced brain metastasis

Though one of the lung cancer cell line (HARA-B) induces bone metastasis [12], it was not known that HARA-B cells also induce brain metastasis. At 3 weeks after the inoculation of HARA-B cells into cardiac ventricle, metastatic foci were mainly found in midbrain-lateral cortex (data not shown). At 4–6 weeks, metastatic foci of various sizes were found throughout the brain. Bigger metastatic foci attracted more astrocytes (Fig. 1a), with the correlation factor of tumor size and GFAP intensity of 0.638 (Fig. 1b). Though the incidence of brain metastasis was different depending on each mouse, the highest incidence was generally observed in cerebral cortex and hippocampus (Fig. 1c). The correlation factor of tumor size and GFAP intensity was higher in hippocampus (0.716) than that in cortex (0.4927) (Fig. 1d). On the other hand, brain's immune cells, including microglia and/or invaded macrophages, also showed accumulation around tumor cells but did not show stronger correlation between tumor size and immune cell population (data not shown). These results suggest that

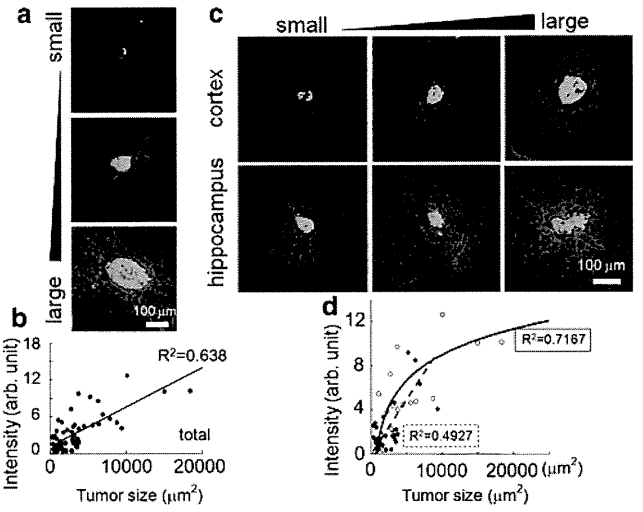

Fig. 1 Astrocyte accumulates around HARA-B cells in vivo. **a** Typical examples of immunostaining of astrogliosis (GFAP) around invaded tumor cells (human cytokeratin, CK). Accumulation of GFAP-positive astrocytes has relation to the size of the tumors. **b** Correlation between tumor size and astrogliosis. Accumulation of astrocytes was indicated as an intensity of GFAP fluorescence. **c** Typical examples of immunostaining indicating more accumulation of astrocytes in hippocampus than in cerebral cortex. **d** Correlation curve between tumor size and GFAP intensity in cortex (*closed circle*) and hippocampus (*open circle*). In hippocampus, astrogliosis around metastatic tumor foci increased logarithmically with correlation factor (R^2) of 0.72

there are correlations between astrocytes and metastatic tumor cells in the microenvironment of brain metastasis.

Effects of astrocytes on the proliferation of HARA-B cells in vitro

In order to elucidate the relationship between astrocytes and HARA-B cells, interaction between 2 cell types was tested in vitro. Primary cultured mouse astrocytes were used and co-cultured with HARA-B cells. The proliferation of HARA-B cells was increased in co-culture with astrocytes in comparison to that in the control (in the absence of astrocytes). In addition, more astrocytes and longer incubation time yielded more proliferation of HARA-B cells (Fig. 2a). The relative increase of proliferation at a ratio of HARA-B cells to astrocytes of 1:5 and 1:10 were 285 ± 9.5% ($n = 6$) and 441 ± 11.2% ($n = 6$), respectively. Since the proliferation of cells in culture system depends on the cell number and physical contact, the effects of conditioned medium on the proliferation of HARA-B cells were examined. First, to avoid physical contact, HARA-B cells were cultured in insert-well with astrocytes in lower-well (ratio of HARA-B to astrocytes was 1:10). After 48 of insert-culture, the medium was collected and added to HARA-B cells and incubated for 48 or 72 h, and then the cell number was counted. Since the

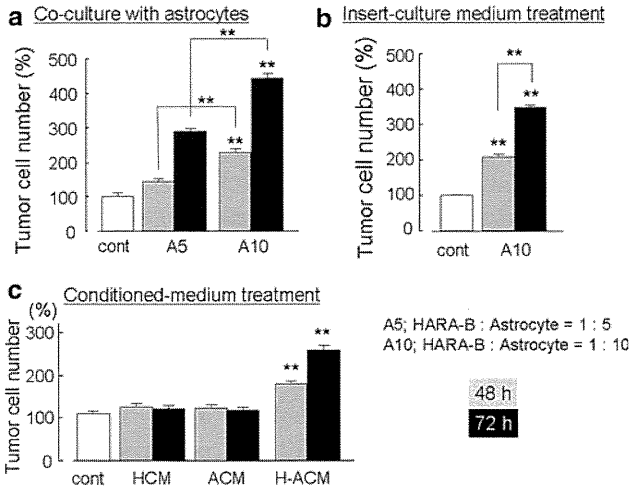

Fig. 2 Astrocyte stimulated the proliferation of tumor cells via soluble factors. **a** The normalized number of HARA-B cells increased according to the ratio of astrocytes to HARA-B cells and incubation time in co-culture treatment (HARA-B cells : astrocytes = 1:5, A5; HARA-B cells : astrocytes = 1:10, A10). **b** Culture medium from insert-culture of astrocytes with HARA-B cells (HARA-B cells : astrocytes = 1:10, A10) significantly increased the proliferation of tumor cells compared to the one without insert-culture medium (control). **c** H-ACM (HARA-B-stimulated astrocyte-conditioned medium), but not HCM (HARA-B-conditioned medium) nor ACM (astrocyte-conditioned medium) significantly increased the proliferation of tumor cells. The incubation time was 48 h (*gray bars*) and 72 h (*black bars*). Each value represents the mean ± SEM (n = 6). ** $P < 0.01$

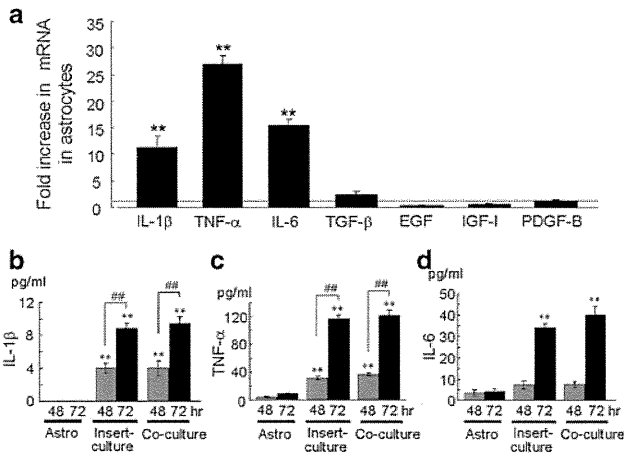

Fig. 3 Expression of mRNA and release of cytokines and growth factors from activated astrocytes. (**a**) Quantitative RT–PCR of IL-1β, IL-6, TNF-α, transforming growth factor-β (TGF-β), insulin-like growth factor-1 (IGF-1), epidermal growth factor (EGF), and platelet-derived growth factor-B (PDGF-B) in astrocytes insert-cultured with HARA-B cells. The expression level of each cytokine or growth factor mRNA was normalized to the level of each cytokine in astrocytes cultured alone. The relative values of each cytokine mRNA in insert-cultured astrocytes for 72 h are shown. Each value represents the mean ± SEM ($n = 3$). Release of IL-1β (**b**), TNF-α (**c**) and IL-6 (**d**) into the culture medium of single-culture of astrocytes (Astro), insert-culture or co-culture of astrocytes and HARA-B cells for 48 and 72 h were detected by ELISA. Each value represents the mean ± SEM ($n = 6$). ** $P < 0.01$, ## $P < 0.01$

medium from insert-culture also increased the proliferation of HARA-B cells, it was suggested that some soluble factors were induced, presumably in astrocytes, without physical cell–cell contact between astrocytes and HARA-B cells (Fig. 2b). Second, it was investigated whether astrocyte-induced soluble factors are constitutive or inducible. Neither astrocyte-conditioned medium (ACM) nor HARA-B-conditioned medium (HCM) but medium from HCM-treated astrocytes (H-ACM) significantly increased the proliferation of HARA-B cells after 48 or 72 h of treatment (Fig. 2c). These results suggest that astrocytes could be stimulated by some soluble factors released from tumor cells, and then produce some growth-promoting factors for tumor cells in turn.

Identification of soluble factors produced by astrocytes

To identify growth-promoting soluble factors produced by astrocytes, mRNA expression of several cytokines and/or growth factors were examined. Activated astrocytes have been shown to produce a wide variety of cytokines including interleukin-1 (IL-1), interleukin-3 (IL-3), interleukin-6 (IL-6), tumor necrosis factor-α (TNF-α), transforming growth factor-β (TGF-β), insulin-like growth factor-1 (IGF-1) and platelet-derived growth factor (PDGF) [6–8]. To discriminate astrocytes-derived cytokines (mouse-origin) from HARA-B-derived cytokines (human-origin), primers for mouse cytokines which do not cross-react to human cytokines were used (Table 1). The amplification of mRNA shows that marked increases in the expression of IL-1β, TNF-α and IL-6 were found in astrocytes after 72 h in the insert-culture with HARA-B cells. The relative expression levels of IL-1β, TNF-α and IL-6 increased to 11.4 ± 2.2, 26.9 ± 1.9 and 15.4 ± 1.1 fold ($n = 3$ each), respectively. On the other hand, expressions of EGF, TGF-β, IGF-I and PDGF-B did not show significant change even after 72 h of the insert-culture with HARA-B cells (Fig. 3a). The RT–PCR for human-IL-1β, human-TNF-α and human-IL-6 in HARA-B cells with or without insert-culture with astrocytes was also performed but the fold increase in mRNA was not significant for either cytokine (data not shown). These results suggest that the origin of IL-1β, TNF-α and mouse-IL-6 were astrocytes but not HARA-B cells.

We also measured the protein levels of mouse-IL-1β, mouse-TNF-α and mouse-IL-6 in the conditioned medium obtained from single-cultured astrocytes (Astro), insert-cultured astrocytes (insert-culture), and co-cultured astrocytes (co-culture) with HARA-B cells after 72 h incubation. Significant increase in the amounts of IL-1β and TNF-α was

observed after 48 and 72 h of insert-culture and co-culture (Fig. 3b, c), while the increase in IL-6 release was only observed after 72 h of insert-culture and co-culture (Fig. 3d). The amounts of each cytokine after 72 h in astrocyte-culture, co-culture, and insert-culture were 0 (not detectable), 8.8 ± 0.7 and 9.4 ± 0.8, pg/ml for IL-1β, 8.3 ± 1.3, 116 ± 5.5 and 121 ± 7.9 pg/ml for TNF-α, and 4.2 ± 1.3, 34.2 ± 1.9 and 40 ± 4.2 pg/ml for IL-6, respectively ($n = 6$).

Effects of recombinant IL-1β, TNF-α and IL-6 and their neutralizing antibodies on the proliferation of HARA-B cells

To confirm the effects of IL-1β, TNF-α and IL-6, recombinant mouse (m) IL-1β, mTNF-α and mIL-6 were applied to HARA-B cells. The concentrations of IL-1β, TNF-α and IL-6 used were employed according to the levels of these cytokines observed in the insert- or co-culture medium (Fig. 3b, c, d). Mouse-IL-1β in a range of 1-10 pg/ml, but not high concentration (50 pg/ml), promoted the proliferation of HARA-B cells (Fig. 4a). Mouse-TNF-α and mIL-6 (10–500 pg/ml each) showed growth-promoting effect on HARA-B cells in a dose-dependent manner (Fig. 4a). These results show that IL-1β, TNF-α and IL-6 released from mouse astrocytes could increase the proliferation of human-origin HARA-B cells.

In reverse, neutralizing antibodies against mIL-1β, mTNF-α and mIL-6 inhibited the effects of co-culture. The titrations of each antibody used (mIL-1β and mTNF-α antibody: 0.2–2.0 μg/ml, mIL-6 antibody: 2.0–20 ng/ml) were determined according to the maximal neutralizing concentration (data not shown). The proliferation of HARA-B cells was promoted to 449 ± 10.2% after co-culture with astrocytes for 72 h in comparison to that in the control (single-culture of HARA-B cells). The antibodies against mIL-1β (1 μg/ml), mTNF-α (1 μg/ml), mIL-6 (10 ng/ml) and all three antibodies were added at 24 h after the co-culture of HARA-B cells with astrocytes, and the co-culture were maintained for further 48 h in the presence of these antibodies. The proliferation of HARA-B cells was significantly attenuated to 149 ± 7.0, 217 ± 10.8, 253 ± 11 and 126 ± 5.9% in the presence of antibodies against IL-1β, TNF-α, IL-6 and all three antibodies, respectively ($n = 5$ each) (Fig. 4b).

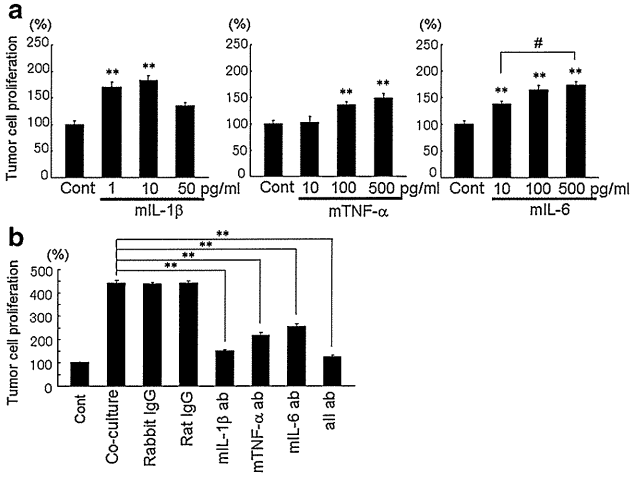

Fig. 4 Effects of recombinant cytokines on HARA-B cell proliferation and inhibitory effects of neutralizing antibodies. **a** Effects of recombinant mouse (m) IL-1β (1–50 pg/ml), mTNF-α (10–500 pg/ml), and mIL-6 (10–500 pg/ml). Data were given as the percentage of tumor cell proliferation without cytokines (without recombinant cytokines; 100%). HARA-B cells were cultured for 24 h in DMEM and then for 48 h in serum free DMEM with each cytokine. Each value represents the mean ± SEM ($n = 6$). **b** Effects of neutralizing antibodies. Anti-mIL-1β (1 μg/ml), anti-mTNF-α (1 μg/ml), anti-mIL-6 (10 ng/ml) neutralizing antibodies, all three antibodies (all ab) and corresponding control IgG were added to co-culture of HARA-B cells and astrocytes. Antibodies were added after 24 h of co-culture of HARA-B cells and astrocytes, and then maintained for 48 h with neutralizing antibodies or control IgG. Data were given as the percentage of control (single-culture of HARA-B cells; 100%) under the same condition without adding antibodies. Each value represents the mean ± SEM (n = 5). ** $P < 0.01$, # $P < 0.05$

Identification of tumor cell-derived factors which activate astrocytes

We then identified HARA-B-derived factors which activate astrocytes and promote expression of IL-1β, TNF-α, and IL-6. The factors in HARA-B cells culture medium was analyzed using the cytokine proteome profiler. The increased expression of cytokines in HARA-B conditioned medium compared to control (10% FBS DMEM) were IL-1ra, IL-2, IL-8, MIF, and SERPINE1 (PAI-1) (Fig. 5a). Among them, IL-8, MIF, and PAI-1 which showed greater expression were tested whether they really activate mouse astrocytes and stimulate the production of IL-1β, TNF-α, and IL-6. The expression of TNF-α mRNAs in astrocytes were significantly increased by recombinant human IL-8 (hIL-8, 10–100 ng/ml) and hMIF (10-100 ng/ml) ($n = 3$ each) (Fig. 5b). The TNF-α mRNA level was not detected with the application of hPAI-1 somehow (not shown). The expression of IL-1β mRNAs in astrocytes were also significantly increased by hIL-8 (100 ng/ml), hMIF (10–100 ng/ml), and hPAI-1 (100–1000 ng/ml) ($n = 3$ each) (Fig. 5c). The expression of IL-6 mRNAs in astrocytes were significantly increased by hMIF (10–100 ng/ml), and hPAI-1 (10–100 ng/ml) but not by hIL-8 ($n = 3$ each) (Fig. 5d). From these results, tumor-derived MIF would be the most potential candidate for stimulating astrocyte and IL-8 and PAI-1 may be less responsible.

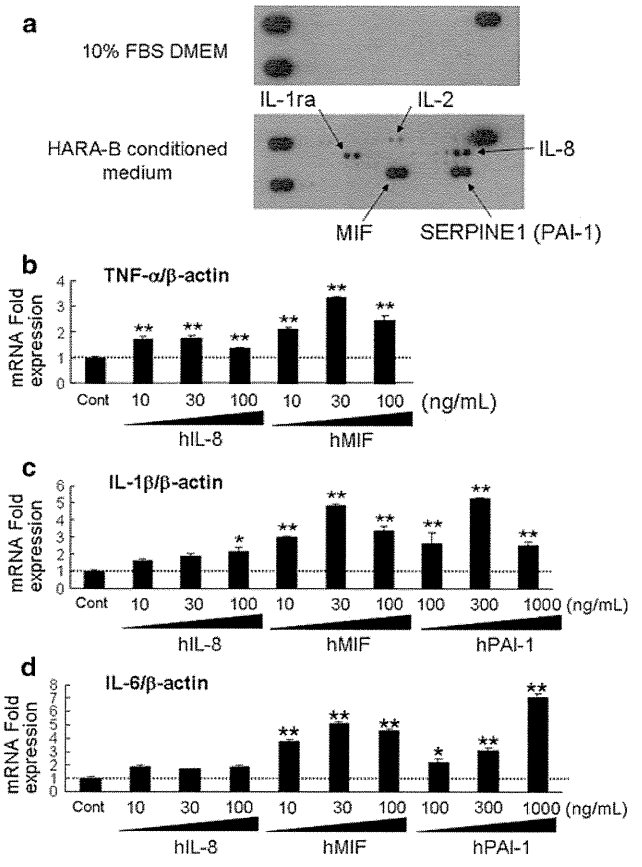

Fig. 5 HARA-B-derived factors which stimulate astrocytes and their effects on expression of mRNA of inflammatory cytokines in astrocytes. **a** Cytokine expression in HARA-B cells culture medium using the proteome profiler. The cytokine expression in medium (10% FBS DMEM) as negative control (*upper panel*) and in HARA-B conditioned medium (*lower panel*), showing the expression of IL-1ra, IL-2, IL-8, MIF, and SERPINE1 (PAI-1). **b–d** Expression of mRNA of inflammatory cytokines (TNF-α, IL-1β, IL-6) in astrocytes treated with each recombinant cytokines (IL-8, MIF, PAI-1). Quantitative RT–PCR of TNF-α (**b**), IL-1β (**c**), and IL-6 (**d**) in astrocytes treated with each cytokine released from HARA-B cells IL-8, MIF, and PAI-1. The expression level of each cytokine was normalized to the level of each cytokine in non-treated astrocytes. The relative values of each cytokine mRNA in astrocyte treated with each cytokine for 72 h are shown. Each value represents the mean ± SEM ($n = 3$). Data of PAI-1-treatment was not shown in TNF-α mRNA

Expression of cytokine receptors on HARA-B cells

The expression of receptors for IL-1β, TNF-α and IL-6 on HARA-B cells were examined by the immunocytochemical staining. Receptors and receptor subunit for these cytokines were detected on cytokeratin-positive HARA-B cells by using antibodies against human-IL-1RtI, human-TNFRtI, human-IL-6Rα and human-gp130. All of these receptors were detected in single-cultures of HARA-B cells (control) (Fig. 6a). To examine the time-dependent change in the expression level for each cytokine receptor and receptor subunit on HARA-B cells, the immunostaining was observed after 24, 48 and 72 h of co-culture with astrocytes. The semi-quantitative analyses showed that the expression level for IL-1RtI and TNFRtI decreased with time after co-culture, while the expression level for IL-6Rα and gp130 were up-regulated in co-culture with astrocytes (Fig. 6b). These results suggest that IL-6 receptors on HARA-B cells may be more functional when HARA-B cells were co-cultured with astrocytes and IL-6 may be the most important cytokine in the promotion of HARA-B cell proliferation in the brain.

Effects of astrocytes on the growth of different lung tumor cell lines in vitro

To test if the mutual stimulation between astrocytes and lung cancer cells was general observation and not specific to HARA-B cells, three other cell lines derived from human squamous cell carcinoma (QG56, EBC-1) and non-small cell lung cancer (PC-9) were examined in vitro. Primary cultured astrocytes, which were prepared from C57BL/6 mice brain, were insert-cultured with other lung tumor cells in the ratio of 1:10 (lung tumor cells : astrocytes). The proliferation of each lung tumor cells increased to 210 ± 27% (QG56, $n = 4$), 480 ± 43% (EBC-1, $n = 4$), and 150 ± 12% (PC9, $n = 4$) after 72 h of incubation with insert-culture medium (ICM), respectively (Fig. 7). These results show that astrocytes, activated by the soluble contact with lung cancer cells, promote not only the growth of HARA-B cells but also that of other lung cancer cells, suggesting that mutual activation of astrocytes and lung tumor cells are common phenomena.

Astrogliosis around human brain metastasis of lung tumor

Since activated astrocytes gathered around brain metastasis in model mice, we examined whether the same pathology was observed in human tissue from brain with lung cancer metastasis. We observed brain metastasis of lung tumor in human tissue sections by Hematoxylin-Eosin staining (Fig. 8a). GFAP-positive astrocytes, which means activated astrocytes, accumulated around metastatic foci (Fig. 8b).

Discussion

Certain cancers, i.e. breast cancer and lung cancer, are liable to metastasize in the brain. The incidence of the brain metastasis has been increasing in recent years [1]. In the metastatic process, the microenvironment of the metastatic sites plays an important role for tumor cells to invade and proliferate in the target tissues [2]. Such a